Nucleic Acids Research, 2026, **54**, gkag598
https://doi.org/10.1093/nar/gkag598
RNA and RNA-protein complexes

OXFORD

rRNA intermediates associate with nucleolar reshaping in *C. elegans*

Jiewei Cheng[1,†], Liang Liu[1,†], Demin Xu[1], Yuxia Chen[2], Yan Kuang[1], Ao Zheng[1], Minjie Hong[1], Xiaona Huang[1], Xiaotian Zhou[1], Wanjing Niu[1], Ji Zhao[2], Xinya Huang[1], Chengming Zhu[2,*], Xiangyang Chen[1,*], Xuezhu Feng[3,*], Shouhong Guang[1,*,‡]

[1]Department of Obstetrics and Gynecology, The First Affiliated Hospital of USTC, The USTC RNA Institute, Ministry of Education Key Laboratory for Membraneless Organelles & Cellular Dynamics, Hefei National Research Center for Physical Sciences at the Microscale, Center for Advanced Interdisciplinary Science and Biomedicine of IHM, School of Life Sciences, Division of Life Sciences and Medicine, University of Science and Technology of China, Hefei, China
[2]School of Life Sciences, Anhui Medical University, Hefei, China
[3]School of Basic Medical Sciences, Anhui Medical University, Hefei, China

*To whom correspondence should be addressed. Email: sguang@ustc.edu.cn
Correspondence may also be addressed to Chengming Zhu. Email: zcm2025@ahmu.edu.cn
Correspondence may also be addressed to Xiangyang Chen. Email: xychen91@ustc.edu.cn
Correspondence may also be addressed to Xuezhu Feng. Email: fengxuezhu@ahmu.edu.cn
†The first two authors should be regarded as Joint First Authors.
‡Lead contact.

Abstract

The nucleolus is a multilayered organelle essential for ribosome biogenesis, yet how ribosomal RNA (rRNA) events coordinate its organization remains unclear. We previously reported that the accumulation of $27SA_2$ pre-rRNA upon class I RPLs (large subunit ribosomal proteins) depletion accompanies the formation of nucleolar rings and vacuoles in *Caenorhabditis elegans*. Here, we systematically investigated the effects of pre-18S rRNA processing and rRNA transcription on nucleolar structure and reported that defects in these molecular events result in reorganization of the nucleolar architecture. Depleting class I RPSs (small subunit ribosomal proteins) induced a concentric three-layered nucleolar architecture, while inhibiting rRNA transcription induced another three-layered sandwich-like nucleolus. During nucleolar reshaping, nucleolar proteins redistributed into distinct subnucleolar compartments. Tracking the subcellular localization of ribosomal DNA (rDNA) via a lacI::tagRFP/lacO system revealed that rDNA also redistributed upon nucleolar reorganization. We identified Ce.22SB pre-rRNA accumulation upon class I RPSs depletion as a key intermediate associated with concentric-spherical nucleoli. Moreover, the conserved nucleolar protein NUCL-1/nucleolin, FIB-1/fibrillarin, and LPD-6/PPAN are essential for nucleolar architecture reorganization and regulates the development of nematodes during impaired rRNA production. Together, these findings demonstrate that nucleolar architecture is associated with the status of rRNA biogenesis and that the accumulation of specific rRNA intermediates correlates with the emergence of distinct nucleolar architectures.

Graphical abstract

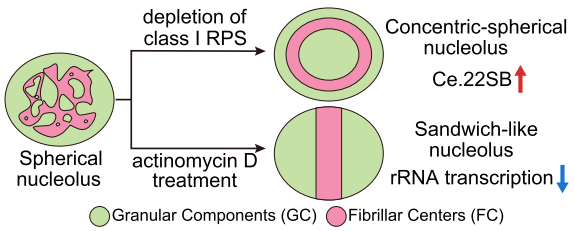

Introduction

Eukaryotic cells achieve spatiotemporal regulation of multiple biochemical reactions through compartmentalized intracellular structures. Among the many subcellular structures, the nucleolus, a multilayered membraneless organelle in the nucleus, serves primarily for ribosomal RNA (rRNA) synthesis and ribosome assembly [1–6]. In eukaryotic cells, two distinct types of nucleolar architectures have been identified, including the tripartite nucleolus and the bipartite nucleolus. The tripartite nucleolus, found in mammals and plants, consists of three internal compartments organized from the periphery to the center: the granular component (GC), the dense fibrillar

Received: August 28, 2025. **Revised:** May 21, 2026. **Accepted:** May 26, 2026

component (DFC), and the fibrillar center (FC), each of which performs specialized functions in rRNA synthesis, rRNA processing, and ribosome assembly, respectively [7–10]. In addition, plant nucleoli typically contain a prominent central nucleolar vacuole (NoV), and the DFC occupies the majority of the nucleolar volume in plant nucleoli [11, 12] (Fig. 1A). In contrast, other eukaryotes, such as *Drosophila* [13], possess a bipartite nucleolus, which lacks a distinct FC layer (Fig. 1A). Similarly, recent studies utilizing superresolution microscopy have revealed that the *Caenorhabditis elegans* nucleolus is also partitioned into two intermingled subcompartments, the FC and GC (Fig. 1A, Type I, wild type) [14].

Despite species-specific structural differences, the mechanisms of ribosome biogenesis are highly conserved among eukaryotes. Insights into ribosome assembly have largely been derived from yeast models, underscoring the universal importance of this process [5, 15, 16]. The nucleolus originates from nucleolar organizer regions (NORs) [2], which consist of ribosomal DNA (rDNA) repeat clusters located primarily on chromosomes I and V in *C. elegans* [17]. The core 47S pre-rRNA is transcribed from rDNA by RNA polymerase I and appears as a characteristic "Christmas tree" structure under electron microscopy, reflecting active transcription. This precursor rRNA is subsequently processed into mature 18S, 5.8S, and 26S rRNAs [18, 19]. In mammals, the transcription of nascent pre-rRNA initiates at the FC-DFC interface and proceeds outward through the nucleolus. As it moves, the rRNA undergoes sequential processing and modification. Continuous production and maturation of rRNA are crucial for preserving both the architecture and the functional dynamics of the nucleolus [20, 21]. Mature ribosomes consist of two unequal subunits: the 40S small subunit (SSU) and the 60S large subunit (LSU). The 40S subunit comprises 18S rRNA and 33 small subunit ribosomal proteins (RPSs), whereas the 60S subunit contains 25S/28S rRNA, 5.8S rRNA, and 47 large subunit ribosomal proteins (RPLs) [22–26].

Ribosome biogenesis is intimately linked to nucleolar structure organization. Perturbations in nucleolar function often manifest as distinct morphological changes. For example, treatment with actinomycin D, an inhibitor of RNA polymerase I, causes the relocation of FC and DFC to the nucleolus periphery and the formation of structures known as nucleolar caps in mammalian cells [27–29]. Nucleolar hypertrophy, which reflects the enhanced ribosomal production required to sustain rapid cell proliferation, has emerged as a hallmark of many tumors [30, 31]. In our previous study, knockdown of the class I *rpl* genes in *C. elegans* led to inappropriate accumulation of the $27SA_2$ pre-rRNA, altered the nucleolar morphology, and resulted in the formation of nucleolar rings and NoVs [3] (Fig. 1A, Type II reshaping). Nucleolar proteins, which are usually involved in rRNA transcription and processing, are excluded from NoVs; nevertheless, nucleoplasmic proteins accumulate in NoVs.

To further investigate the regulation of nucleolar structure organization, we examined whether deficient RPS proteins and impaired rRNA production would also induce nucleolar reshaping or nucleolar architecture alteration in *C. elegans*. Unlike the formation of NoVs, which is induced by class I *rpl* knockdown [3], we observed two striking nucleolar morphologies, concentric-spherical nucleoli (Fig. 1A, Type III reshaping) and sandwich-like nucleoli ((Fig. 1A, Type IV reshaping). Concentric-spherical nucleoli are induced by the knockdown of 11 particular RPS proteins, which are termed class I RPSs. Interestingly, after the class I RPS proteins were knocked down, the Ce.22SB pre-rRNA consistently accumulated. Moreover, the proteins involved in rRNA transcription as well as 18S and 26S rRNA processing are separated into particular nucleolar subcompartments. The formation of sandwich-like nucleoli is induced by actinomycin D treatment, in which rRNA transcription as well as 18S and 26S rRNA processing factors also redistribute into distinct nucleolar subcompartments. We identified NUCL-1 as a key factor in nucleolar structure reorganization and as a checkpoint that promotes the development of *C. elegans* under conditions of impaired rRNA processing. These findings highlight the critical interplay between nucleolar architecture and rRNA biogenesis and underscore the importance of nucleolar structure integrity for organismal fitness.

Materials and methods

Strains

The Bristol strain N2 was used as the standard wild-type strain. All strains were grown at 20°C unless otherwise specified. The strains used in this study are listed in Supplementary Table S1.

RNAi

RNAi experiments were performed at 20°C by placing synchronized embryos on feeding RNAi plates as previously described [32]. HT115 bacteria expressing the empty vector L4440 (a gift from A. Fire) were used as controls (EV, empty vector). Bacterial clones expressing double-stranded RNAs (dsRNAs) were obtained from the Ahringer RNAi library [33] and sequenced to verify their identity. Some bacterial clones, which are listed in Supplementary Table S2, were constructed in this work.

Imaging

Animals were immobilized in ddH_2O containing 0.5 M sodium azide and mounted on glass slides (Citotest, 80302-0004) with coverslips (Citotest, 80340-1630) prior to imaging. Images were acquired using a Leica upright DM4 B microscope equipped with a Leica K5 sCMOS microscope camera and an HC PL FLUOTAR 100x/1.40–0.70 oil objective. Image acquisition and processing were performed using Leica Application Suite X software (version 3.7.4.23463), and images were further rotated and cropped using Adobe Photoshop CS6. Unless otherwise specified, all worms were imaged at the L3–L4 stage.

Construction of plasmids and transgenic strains

For the ectopic transgenes, the promoter and CDS regions and UTRs were amplified from N2 genomic DNA. A GFP::3xFLAG sequence was PCR (polymerase chain reaction) amplified from SHG326 genomic DNA. The mCherry coding sequence was amplified from pFCJ90. The vector fragment was PCR amplified from the plasmid pSG274. These fragments were joined together by Gibson assembly to form the repair plasmid with the ClonExpress MultiS One Step Cloning Kit (Vazyme Biotech, Nanjing, China, Cat. No. C113-01/02). The transgene was integrated into *C. elegans* chromosomes I and II via a modified counterselection (cs)-CRISPR (Clustered Regularly Interspaced Short Palindromic Repeats)

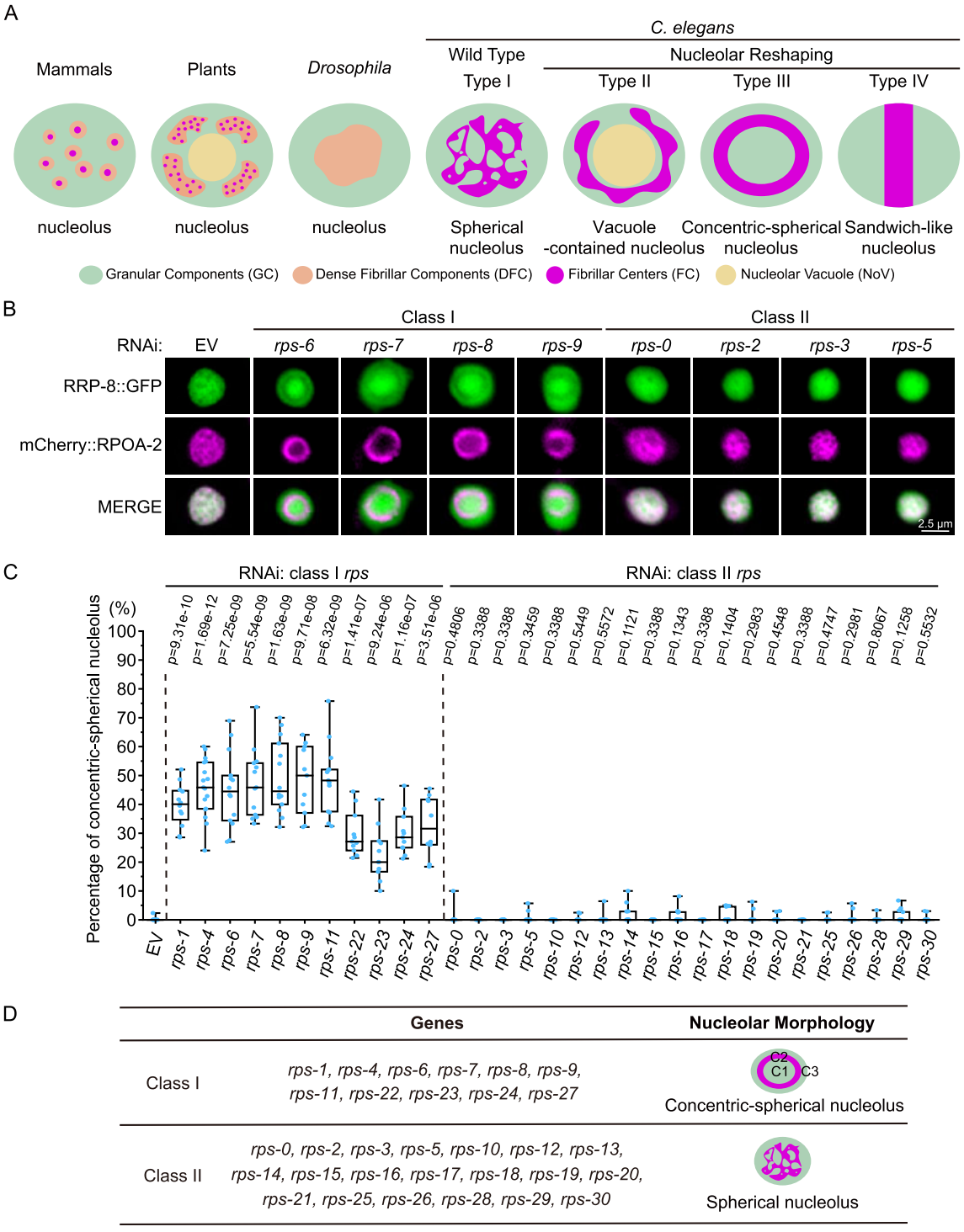

Figure 1. Knocking down class I *rps* genes induces nucleolar reorganization. (**A**) Schematic diagram of nucleolar organization in mammals, plants, *Drosophila*, and *C. elegans*, including three types of nucleolar reshaping. (**B**) Fluorescence microscopy images of *C. elegans* nucleoli in hypodermal cells after the indicated genes were knocked down via RNAi (RNA interference). EV, empty vector. All worms were imaged at the L3–L4 stage. Scale bar, 2.5 μm. (**C**) Quantification of concentric-spherical nucleoli after RNAi knockdown of the indicated genes. Each box represents data from at least 11 worms, each dot represents the proportion of concentric-spherical nucleoli observed in at least 9 individual hypodermal cells from a single worm. Significance was tested with two-tailed Student's *t*-test. (**D**) Summary of concentric-spherical nucleoli formation upon the knockdown of class I and II *rps* genes.

method [34, 35]. The sequences of the primers are listed in Supplementary Table S3.

For *in situ* knock in transgenes, the 3xFLAG::GFP coding region was PCR amplified from SHG1248 genomic DNA. The GFP:3xFLAG coding region was PCR amplified from SHG2123 genomic DNA. The mCherry coding region was PCR amplified from SHG1660 genomic DNA. The tagRFP coding region was PCR amplified from YY1446 genomic DNA. The homologous left and right arms (1.5 kb) were PCR amplified from N2 genomic DNA. The backbone was PCR amplified from the plasmid pCFJ151. All these fragments were joined together by Gibson assembly to form the repair plasmid with the ClonExpress MultiS One Step Cloning Kit (Vazyme Biotech, Nanjing, China, Cat. No. C113-01/02). This plasmid was coinjected into N2 animals with three sgRNA expression vectors, 5 ng/ml pCFJ90, and the Cas9 II-expressing plasmid. The sequences of the primers are listed in Supplementary Table S4.

Actinomycin D treatment

Actinomycin D (MedChemExpress no. HY-17559, CAS:50-76-0) was prepared at 20 mg/ml in DMSO (Dimethyl sulfoxide) as a stock solution. Each 10.5 μl of actinomycin D stock solution was diluted with 300 μl of concentrated OP50 and layered onto NGM plates. Synchronized embryos were placed onto the seeded plates and grown for 48 h before imaging.

BMH-21 treatment

BMH-21 (MedChemExpress no. HY-12484, CAS:896705-16-1) was prepared at 20 mg/ml in DMSO as a stock solution. Each 35 μl of BMH-21 stock solution was diluted with 300 μl of concentrated OP50 and layered onto NGM plates. Synchronized embryos were placed onto the seeded plates and grown for 48 h before imaging.

Fluorescence recovery after photobleaching

FRAP (fluorescence recovery after photobleaching) experiments were performed via a Zeiss LSM980 laser scanning confocal microscope at 20°C. Worms were anesthetized with 2 mM levamisole. A region of interest was bleached with 100% laser power for 3–4 s, and the fluorescence intensities in these regions were collected every 5 s and normalized to the initial intensity before bleaching. For analysis, image intensity was measured as the mean and further analyzed with GraphPad Prism 10.0 software.

cRT-PCR

L3–L4 stage worms were incubated with TRIzol (Invitrogen) reagent followed by seven quick liquid nitrogen freeze–thaw cycles. RNA was precipitated with isopropanol followed by DNaseI digestion (Thermo Fisher). Two micrograms of total RNA was circularized with a T4 RNA Ligase 1 Kit (M0204. NEB) and then purified with TRIzol reagent followed by isopropanol precipitation. The circularized RNA was reverse transcribed via the GoScript Reverse Transcription System (Promega #A5001). PCR was performed via 32 cycles of 2X Phanta Flash Master Mix (Vazyme, P520-AA). The primer sets used in cRT-PCR (circularized reverse-transcription PCR) are listed in Supplementary Table S5.

Quantitative real-time PCR

All quantitative real-time PCR (qPCR) experiments were performed via a Roche system. Complementary DNA (cDNA) was quantified with SYBR Green Master Mix (Vazyme, Q111-02), and qPCR was performed according to the vendor's instructions. The primer sets used in this work are listed in Supplementary Table S6.

RNA immunoprecipitation followed by quantitative PCR

L3–L4 stage worms were collected and washed with M9 buffer, followed by lysis in RIP lysis buffer containing RNase inhibitors and protease inhibitors. The lysates were clarified by centrifugation, and an aliquot was reserved as input. The remaining lysate was incubated with anti-FLAG M2 magnetic beads (Sigma, M8823) at 4°C with rotation. After incubation, the beads were washed four times and RNA was extracted using TRIzol reagent followed by isopropanol precipitation. cDNAs were generated from RNA using HiScript III RT SuperMix for qPCR (Vazyme, R323), which includes a random primer/oligo(dT)20VN primer mix for reverse transcription. qPCR was performed as described above. The primers used for RIP-qPCR (RNA immunoprecipitation followed by quantitative PCR) are listed in Supplementary Table S7. Enrichment of RNA in the immunoprecipitated samples was calculated relative to input RNA.

Stage distribution

Five gravid adults were allowed to lay eggs for 1 h on the indicated RNAi plates and then removed. The developmental progress was then monitored after 96 h at 20°C.

Statistics

Statistics Boxplots are presented with medians and minimums and maxima. Bar graphs with error bars are presented, which present the means and standard deviations (SDs). All experiments were conducted with independent *C. elegans* animals at the indicated number of times (*N*). Statistical analysis was performed with a two-tailed Student's *t*-test.

Results

Knocking down class I *rps* genes induces nucleolar reorganization

Ribosomes are composed of two conserved subunits, the LSU and the SSU, which are primarily composed of RPL and RPS, respectively [22–24, 26, 36]. Both RPS and RPL proteins are engaged in various processing and maturation steps of 18S, 5.8S, and 26S rRNAs. Our previous study explored the role of RPL proteins in nucleolar morphology regulation and revealed that the knock down of class I RPL proteins leads to nucleolar reshaping, in which the spherical nucleolus (Type I, wild type) is transformed into a ring-shaped and vacuole-contained nucleolus (Type II reshaping) (Fig. 1A and 2A) [3]. To investigate whether RPS proteins have similar impacts on nucleolar morphology, we constructed an RRP-8::GFP;mCherry::RPOA-2 strain and treated nematodes with dsRNAs targeting the *rps* genes. RRP-8 is an rRNA processing factor involved in the N1-methyladenosine (m1A) modification of 26S rRNA [37]. RPOA-2 is the subunit of RNAP I [38]. Both RRP-8 and RPOA-2 localize to the nucleolus.

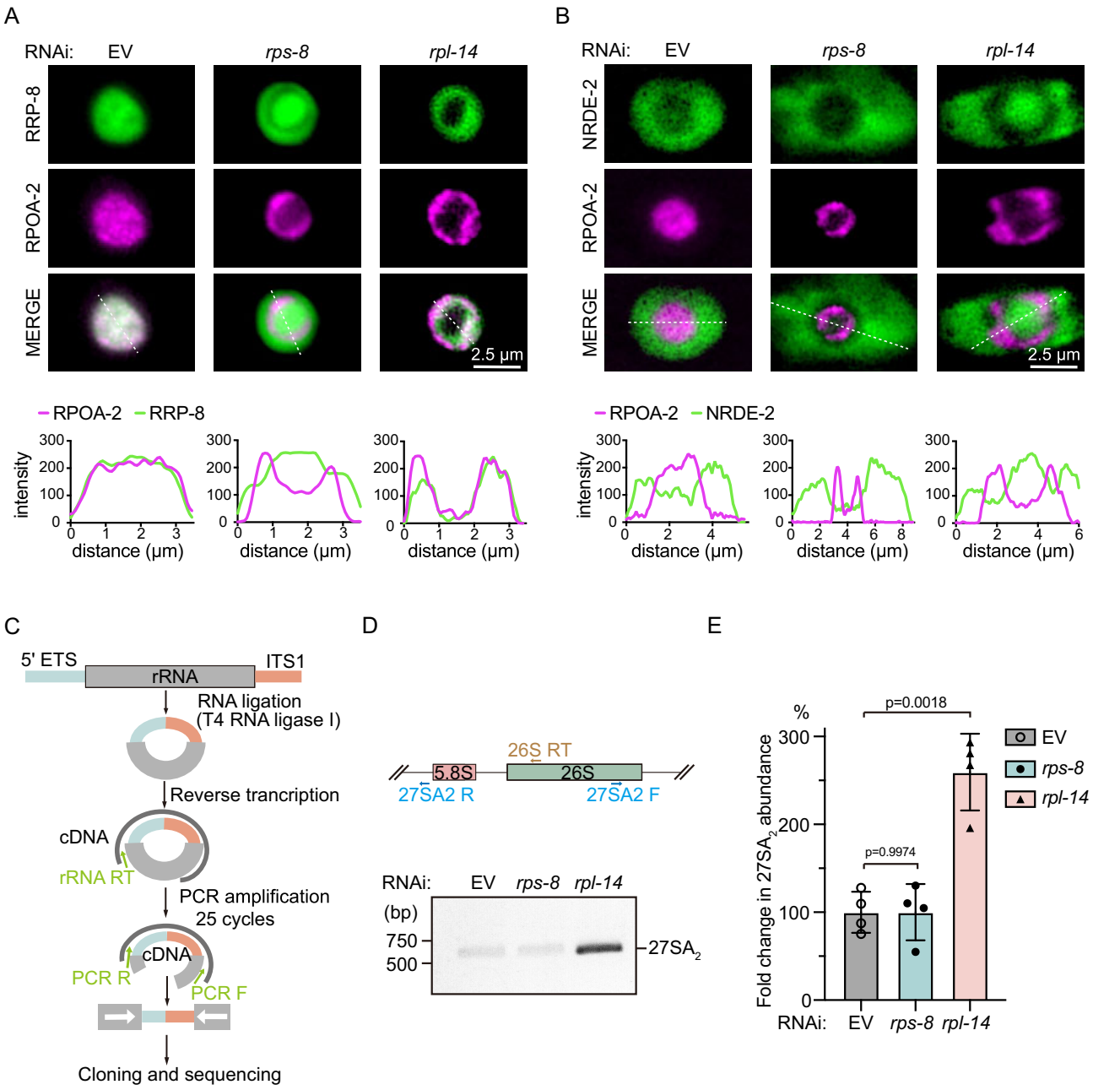

Figure 2. Differential nucleolar structures following the knockdown of class I RPS and class I RPL proteins. (**A**) (top) Fluorescence microscopy images of *C. elegans* nucleoli in hypodermal cells after the indicated genes were knocked down via RNAi. Scale bar, 2.5 μm. (bottom) Fluorescent density scan of RRP-8::GFP and mCherry::RPOA-2 in the indicated lines via ImageJ. (**B**) (top) Fluorescence microscopy images of *C. elegans* nucleoli in hypodermal cells after the indicated genes were knocked down via RNAi. Scale bar, 2.5 μm. (bottom) Fluorescent density scan of GFP::NRDE-2 and mCherry::RPOA-2 of the indicated lines via ImageJ. (bottom of A and B) A line was drawn across the nucleolus, and fluorescence intensity along the line was measured by ImageJ to generate a profile plot. The *y*-axis represents fluorescence intensity, and the *x*-axis represents the distance along the line. (**C**) Schematic diagram of the circularized reverse-transcription PCR (cRT-PCR) method. (**D**) cRT-PCR assay and (**E**) quantification of $27SA_2$ pre-rRNA after knocking down the indicated genes via RNAi. The data are presented as the mean ± SD of four biological replicates. Statistical significance was assessed via a two-tailed *t*-test.

Upon the knockdown of the 31 *rps* genes, distinct alterations in nucleolar morphology were observed in hypodermis. On the basis of the relative changes in the localization of RRP-8 and RPOA-2 in hypodermal cells, we categorized the *rps* genes into two classes (summarized in Fig. 1D). The class I *rps* genes include 11 members, including *rps-1 and rps-4*. RNAi-mediated depletion of the class I *rps* genes induced nucleolar reshaping characterized by a concentric, three-layer architecture (Fig. 1B and Supplementary Fig. S1A), including the innermost C1 (concentric-spherical nucleolus-1), middle C2, and outermost C3 layers (Fig. 1D). For nomenclature, we named the three-layer nucleolus the concentric-spherical nucleolus (Type III reshaping). While RRP-8 preferentially localized in the C1 and C3 layers, RPOA-2 exclusively accumulated in the C2 layer after knocking down class I *rps*. The class II *rps* genes include 20 members, including *rps-0 and rps-2*. We

did not observe noticeable patterns in the nucleolar structure after RNAi was used to target the class II *rps* genes (Fig. 1B and C, and Supplementary Fig. S1A).

In the germline, depletion of *rps* caused pronounced atrophy and morphological disruption, making nucleolar organization difficult to be reliably assessed. In intestinal cells, depletion of class I *rps* genes resulted in a modest proportion of concentric-spherical nucleoli. We examined 400 cells and detected ∼2%–7% cells displayed concentric-spherical nucleoli, but none in control animals (Supplementary Fig. S1B). We speculated that the distinct ploidy and transcriptional demands of intestinal cells [39] may limit the accumulation of rRNA intermediates to sufficient levels to trigger nucleolar reshaping. Together, these observations suggest that nucleolar reshaping may vary across different tissue types.

Class I RPS and class I RPL proteins act differently in organizing nucleolar architecture

Previously, we showed that upon RNAi targeting class I RPL proteins, RPOA-2-marked nucleoli exhibit a ring-shaped morphology that surrounds the NoV [3, 14]. Here, we also observed a ring-shaped distribution of RPOA-2 after RNAi targeting class I RPS proteins. To distinguish these two rings, we used RNAi to knock down *rps-8* (class I *rps*) and *rpl-14* (class I *rpl*) in the RRP-8::GFP;mCherry::RPOA-2 strain. In control animals not subjected to RNAi, both RRP-8 and RPOA-2 were largely distributed in the spherical nucleolus (Fig. 2A). RNAi targeting *rps-8* induced a three-layer nucleolar architecture, in which RRP-8 accumulated in the innermost C1 and outermost C3 layers, but RPOA-2 accumulated in the middle C2. Knockdown of *rpl-14* resulted in a two-layered nucleolus, in which the nucleolar proteins accumulated in the outside ring and the nucleoplasmic proteins occupied the inside NoV [3]. Both RRP-8 and RPOA-2 accumulated in the ring-shaped nucleolus but were excluded from the NoV layer (Fig. 2A), suggesting that the two rings induced by *rps-8* and *rpl-14* RNAi are different.

Similarly, we used RNAi to target *rps-8* and *rpl-14* in a GFP::NRDE-2;mCherry::RPOA-2 strain. NRDE-2 functions in nuclear and nucleolar RNAi and typically resides in the nucleoplasm [40–42]. Following *rpl-14* RNAi, NRDE-2 accumulated in both the nucleoplasm and the NoV (Fig. 2B). In contrast, upon *rps-8* knockdown, NRDE-2 remained predominantly in the nucleoplasm and did not redistribute into the nucleolus (Fig. 2B).

To further confirm that the generation of ring-shaped nucleolar structures is different under these two conditions, we used cRT-PCR [43] to assay the $27SA_2$ pre-rRNA, the increase in which promotes nucleolar reshaping and the formation of NoV [3]. Knockdown of *rpl-14* induced the accumulation of $27SA_2$ pre-rRNA, as previously reported [3]. However, we did not detect the accumulation of $27SA_2$ pre-rRNA after knocking down the class I *rps* gene *rps-8* (Fig. 2C–E). In addition, although vacuole-containing nucleoli are observed in normal growing animals [3], concentric-spherical nucleoli are rarely noticeable under normal laboratory culture conditions. Together, these results indicate that NoVs (Type II reshaping) and concentric-spherical nucleoli (Type III reshaping) represent two distinct modes of nucleolar reshaping that likely arising from different underlying mechanisms.

Distinct redistribution patterns of nucleolar proteins during nucleolar reorganization

The redistribution of RRP-8 and RPOA-2 upon the knockdown of class I RPS proteins suggested that other nucleolar proteins may also exhibit diverse characteristics during the reorganization of the nucleolar architecture. To investigate the subcellular localization of nucleolar proteins during the formation of concentric-spherical nucleoli, we used CRISPR/Cas9 technology to generate single-copy transgenes of a number of nucleolar proteins (Supplementary Fig. S2A). The construction details of each strain used in this study are provided along with the corresponding source references.

Nucleolar proteins are involved in various steps of rRNA biogenesis, including rRNA transcription, ribosome assembly, pre-rRNA processing, and maturation. RPOA-1, RPOA-2, and RPAC-19 are subunits of the RNA polymerase I complex [3, 38, 41]. DAO-5 is an rRNA transcription factor [4, 44]. Upon knockdown of *rps-8*, RPOA-1, RPOA-2, RPAC-19, and DAO-5 similarly accumulated in the middle C2 layer (Fig. 1B and 3A, and Supplementary Fig. S2B and C). RBD-1, an 18S rRNA processing factor [3, 45], also localized to the C2 layer upon *rps-8* RNAi (Fig. 3B). FIB-1 encodes the *C. elegans* ortholog of human fibrillarin and *Saccharomyces cerevisiae* Nop1p [46], which is an essential factor for 18S rRNA processing [3, 47]. GARR-1 encodes the *C. elegans* ortholog of human GAR1 [4, 48]. FIB-1 and GARR-1 normally reside in the FC region [14], with GARR-1 showing predominant nucleolar localization. Both FIB-1 and GARR-1 accumulated in the middle C2 layer after *rps-8* RNAi (Fig. 3C and Supplementary Fig. S2D). RRP-8 is involved in the m1A modification of 26S rRNA [37, 49]. T06E6.1 is an ortholog of human WDR74 and may be involved in ribosomal large subunit biogenesis [3, 50]. Both RRP-8 and T06E6.1 accumulated in the C1 and C3 layers upon *rps-8* RNAi (Fig. 1B and 3D). NUCL-1 encodes an evolutionarily conserved protein that is highly homologous to yeast and human nucleolin [3, 51]. LPD-6 is an ortholog of human PPAN-P2RY11 and yeast Ssf1 and is required for ribosomal large subunit maturation [52–54]. NUCL-1 and LPD-6 reside in the GC region in control animals and accumulated in the C1 and C3 layers upon *rps-8* RNAi (Fig. 3E and Supplementary Fig. S2E). The results are summarized in Fig. 3F and indicate that the factors involved in rRNA transcription, 18S rRNA processing, and the FC accumulate in the C2 layer, whereas the proteins required for 26S rRNA processing, ribosome large subunit assembly and the GC accumulate in the C1 and C3 layers after nucleolar reshaping.

To ensure that these phenotypes reflect genuine nucleolar reshaping rather than artifacts arising from fluorescence tagging, we employed a split-GFP strategy to visualize the endogenous protein in the somatic cells. Using CRISPR/Cas9-mediated genome editing, a small 16-amino acid split superfolder-GFP11 tag (sGFP11) was inserted at the C-terminus of endogenous NUCL-1, generating the NUCL-1::sGFP11 allele in a strain carrying *eft-3p::sGFP(1–10)::unc-54UTR*, which drives sGFP(1–10) expression in the hypodermis. Although this strategy improved the baseline resolution [14], the nucleolar phenotypes observed using the split-GFP strain were largely indistinguishable from those observed using the NUCL-1::GFP strain upon *rps* knockdown (Supplementary Fig. S2F), indicating that the mesoscale nucleolar structural changes do not depend on the tagging strategy.

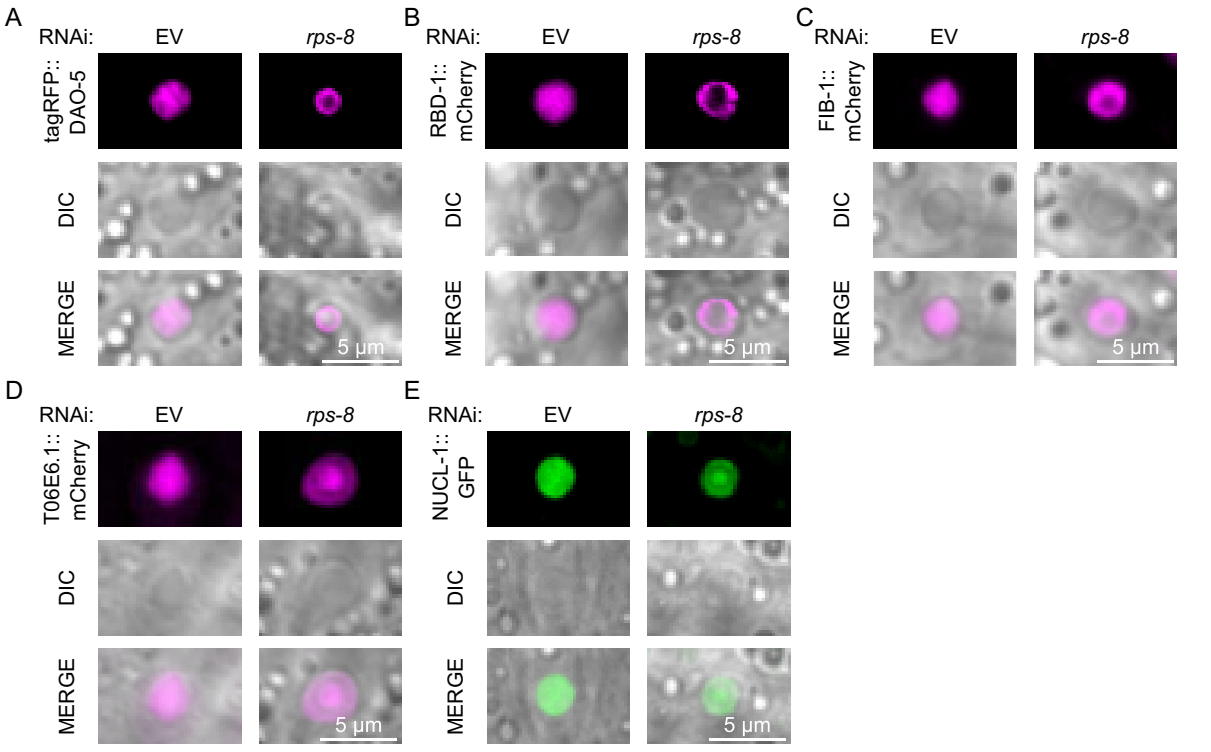

F

Nucleolar structure		Location	Proteins	Function
Spherical	Concentric-spherical			
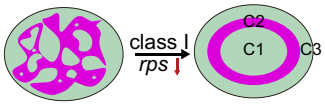		C2	RPOA-1 RPOA-2 DAO-5 RPAC-19	Transcription factor
			RBD-1	18s rRNA processing
			FIB-1 GARR-1	Fibrillar center
		C1&C3	RRP-8	26s rRNA N1-methyladenosine modification
			T06E6.1	Ribosomal large subunit biogenesis
			NUCL-1 LPD-6	Granular center

Solid line outlines the nucleolus

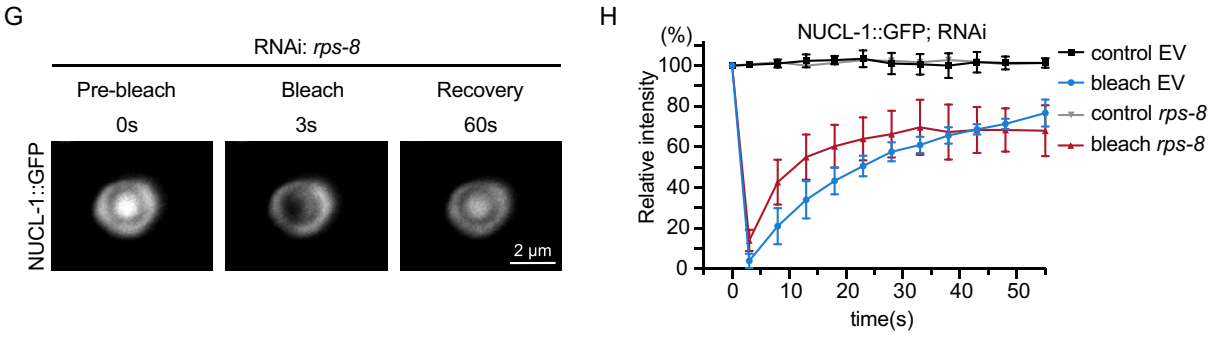

Figure 3. Distinct redistribution patterns of nucleolar proteins during nucleolar reorganization. (**A**–**E**) DIC and fluorescence microscopy images of the indicated transgene after knocking down *rps-8*. Scale bar, 5 μm. (**F**) Summary of the localization of the indicated proteins after *rps-8* RNAi. (**G**) FRAP assay of the NUCL-1::GFP transgene in the indicated regions after *rps-8* knockdown. Scale bar, 2 μm. (**H**) Quantification of FRAP data. Mean ± SD, $n = 3$ independent animals.

Phase separation of nucleoli is essential for nucleolar function [7]. We performed a FRAP assay to investigate whether nucleolar reshaping alters the mobility of rRNA transcription and processing factors by comparing the mobility of NUCL-1 and GARR-1 in both spherical and concentric-spherical nucleoli. In the concentric-spherical nucleoli induced by *rps-8* knockdown, NUCL-1 marked the C1 and C3 layers, whereas GARR-1 marked the C2 layer. In control and *rps-8*-knockdown animals, both NUCL-1 and GARR-1 exhibited similar mobility (Fig. 3G and H, and Supplementary Fig. S2G and H). These data suggested that type III reshaping may not affect the mobility of the components for rRNA transcription and processing.

The Ce.22SB pre-rRNA accumulates upon the knockdown of class I RPS proteins

RPS proteins are 40S ribosome subunits that are involved in 18S rRNA processing and small ribosome assembly [24, 26, 55]. We used cRT-PCR to assay pre-18S rRNA via primer sets targeting the external transcribed spacer (ETS) [56] upon knocking down *rps* genes (Fig. 4A and B). We identified four distinct bands, which were subsequently cloned and verified via Sanger sequencing (Supplementary Fig. S3A–F). Based on size estimation and comparison with pre-rRNA processing pathways in *S. cerevisiae*, several intermediates were tentatively assigned as yeast-like species (e.g. 22S-, 21S-, and 20S-like) (Supplementary Fig. S3A–G) [57–59]. The prefix "Ce" indicates that these assignments are specific to *C. elegans*. We next defined cleavage site annotations analogous to those established in yeast (A0, A1, A2, and A3) [57–59]. Two putative TATA-like elements were identified at 420 and 396 bp upstream of the 18S rRNA-coding sequence [45]. Transcription likely initiates downstream of the second TATA-like element, which we designate as the A0 site [−394 (18S)] (Supplementary Fig. S3A and B). The A1 site defines the 5′ end of 18S rRNA. Moreover, we mapped cleavage sites A2 and A3 to positions +245 (18S) and +376 (18S), respectively (Supplementary Fig. S3A–F). These regions within ITS1 likely correspond to those previously defined as "III" and "IV" by Saijou *et al.* and Shovon *et al.* via northern blotting and primer extension analyses, respectively [45, 60]. Based on these combined analyses, the four bands were designated as Ce.22SA, Ce.22SB, Ce.21S, and Ce.20S (Fig. 4A and B). In addition, we identified an alternative cleavage site located 16 nt upstream of the canonical A1 position, termed A1′ (Supplementary Fig. S3E and F). Due to the close proximity between A1 and A1′, they are not resolved as separate bands in the cRT-PCR gel electrophoresis. Intermediates generated from this upstream cleavage site were designated as Ce.21S′ and Ce.20S′, representing distinct variants of the corresponding Ce.21S and Ce.20S species (Fig. 4B and Supplementary Fig. S3E and F). For simplicity, these intermediates are collectively annotated as Ce.21S or Ce.20S.

Strikingly, the knockdown of class I *rps* consistently led to the accumulation of both Ce.22SA and Ce.22SB pre-rRNAs, whereas the knockdown of class II *rps* had a subtle effect on their levels (Fig. 4C and D, and Supplementary Fig. S4A). A few other *rps* genes, including *rps-5*, *rps-13*, and *rps-28*, which are not class I *rps genes*, still accumulated Ce.22SA pre-rRNA but not Ce.22SB pre-rRNA. Taken together, these data suggest that inappropriate accumulation or processing of Ce.22SB pre-rRNA is closely associated with the formation of concentric-spherical nucleoli.

Interestingly, the classification of *rps* genes in *C. elegans* is coincidentally consistent with the classification of *rps (i-rps/p-rps)* genes in human cells [61] (Supplementary Fig. S4B). In HeLa cells, knockdown of i-RPS leads to the accumulation of 45S and 30S pre-rRNAs due to defects in processing steps within the 5′ ETS and internal transcribed spacer 1 (ITS1). This perturbation is accompanied by irregular nucleolar morphology and disorganization of perinucleolar chromatin. For example, depletion of RPS16 results in smaller, rounded nucleoli [61]. In *C. elegans*, the accumulation of Ce.22SB pre-rRNA also arises from the failure of processing steps in 5′ ETS and ITS1 regions. These findings imply the critical roles of RPS proteins in rRNA biogenesis, ribosome assembly, and nucleolar architecture.

To further test whether Ce.22SB pre-rRNA accumulation is functionally linked to the formation of concentric-spherical nucleoli, we perturbed additional factors involved in 40S ribosome subunits processing, including those required for early rRNA cleavage and maturation (Supplementary Fig. S5A). Depletion of several of these factors also led to the formation of concentric-spherical nucleoli and increased the accumulation of Ce.22SB pre-rRNA (Supplementary Fig. S5B–D). For example, POPL-5, which participates in A3 cleavage, produced both phenotypes upon its knockdown by RNAi. We note that Ce.22SB pre-rRNA accumulation was measured at the whole-organism level, whereas nucleolar reshaping was most prominent in hypodermal cells. Nevertheless, the consistent concordance observed across multiple independent perturbations supports a close association between Ce.22SB pre-rRNA accumulation and concentric-spherical nucleolar formation.

Inhibition of rRNA transcription induces the formation of sandwich-like nucleoli

We then tested whether and how the reduction in rRNA levels impacts the nucleolar architecture by using actinomycin D to inhibit rRNA transcription. Our previous work revealed that actinomycin D inhibits the accumulation of $27SA_2$ pre-rRNA and prevents the formation of NoV [3].

We treated the RRP-8::GFP;RPOA-2::mCherry strain with 30 μg/ml actinomycin D and visualized the nucleolar substructure. Upon actinomycin D treatment, the pre-rRNA levels decreased (Supplementary Fig. S6A). RRP-8 and RPOA-2 underwent type IV nucleolar reshaping, forming sandwich-like nucleoli (Fig. 5A and Supplementary Fig. S6B), which is distinct from the concentric-spherical nucleolus, yet maintained a similar layered organization, with RRP-8 occupying the outside layers S1 and S3 (sandwich-like nucleoli-1 and -3) and RPOA-2 accumulating in the middle S2 layer. The classification of nucleolar proteins in actinomycin D-induced reshaping is consistent with the classification observed upon class I *rps* knockdown (Fig. 5C–G and Supplementary Fig. S6C–F and summarized in Fig. 5B). The factors involved in rRNA transcription, 18S rRNA processing, and FC organization, such as GARR-1, FIB-1, RPOA-1, RPOA-2, DAO-5, RPAC-19, and RBD-1, are localized to the sandwich core (S2). The outer layers of the sandwich-like nucleolar structure (S1 and S3) were enriched with proteins required for 26S rRNA processing, large subunit assembly, and GC organization, including NUCL-1, LPD-6, RRP-8, and T06E6.1. Moreover, worms

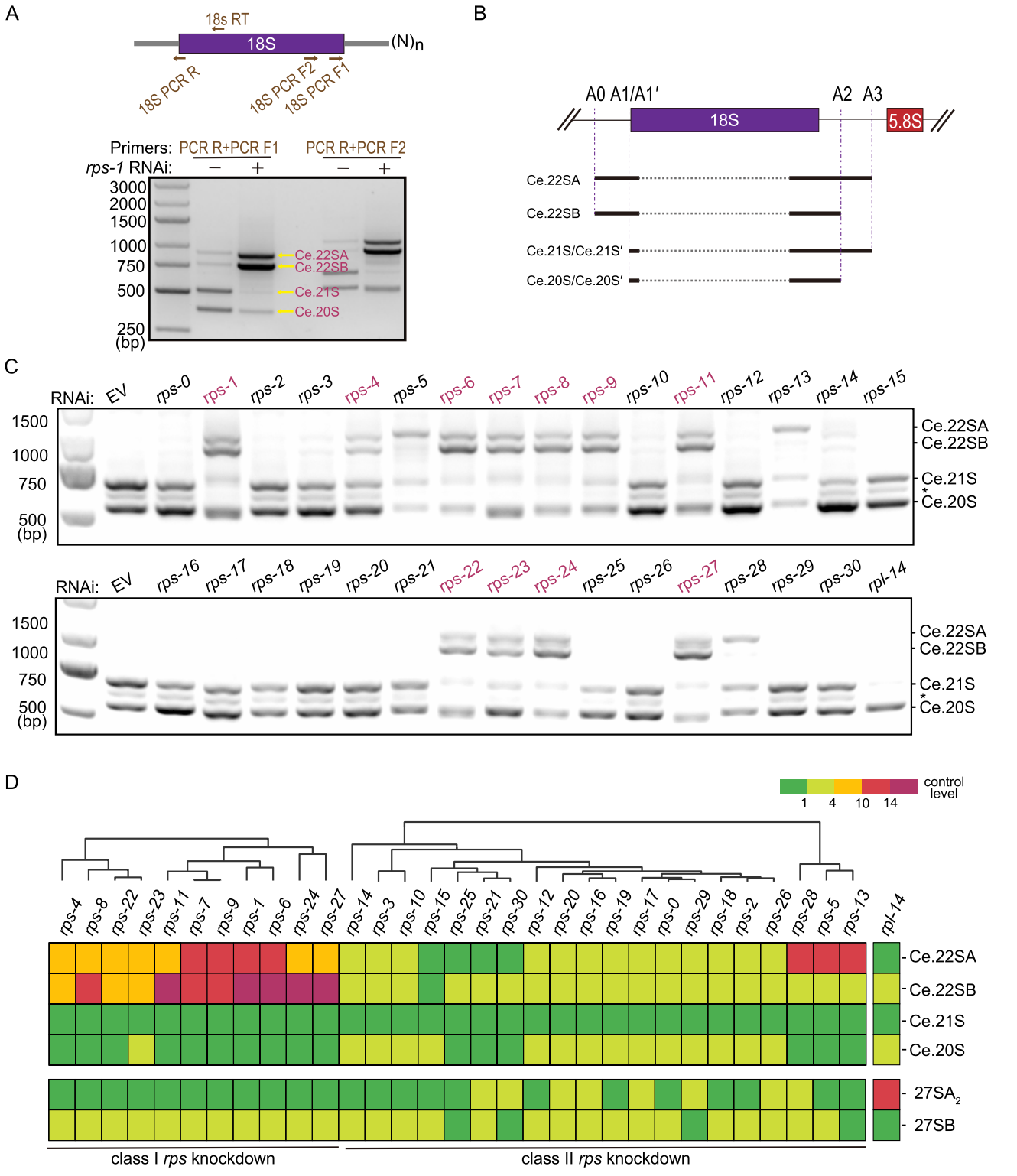

Figure 4. Knocking down class I RPS proteins induces the accumulation of the Ce.22SB pre-rRNA. (**A**) cRT-PCR assay and (**B**) schematic diagram of pre-18S rRNA. (**C**) cRT-PCR assay of pre-18S rRNA after knocking down the indicated *rps* genes via RNAi. Class I *rps* genes are shown in rich carmine. Primer pair 18S PCR F2 and 18S PCR R was used for amplification. Four major bands were identified. An additional weak band (indicated by an asterisk) migrating below Ce.21S was detected. This band likely represents a chimeric product of Ce.21S and Ce.20S pre-rRNAs based on sequencing. (**D**) Quantification of pre-18S and pre-26S rRNA (Fig. 4C and Supplementary Fig. S4A, respectively) via ImageJ after knocking down the indicated *rps* genes via RNAi and normalization to the corresponding intermediates in EV RNAi controls. Hierarchical clustering analysis was performed on the basis of the normalized values.

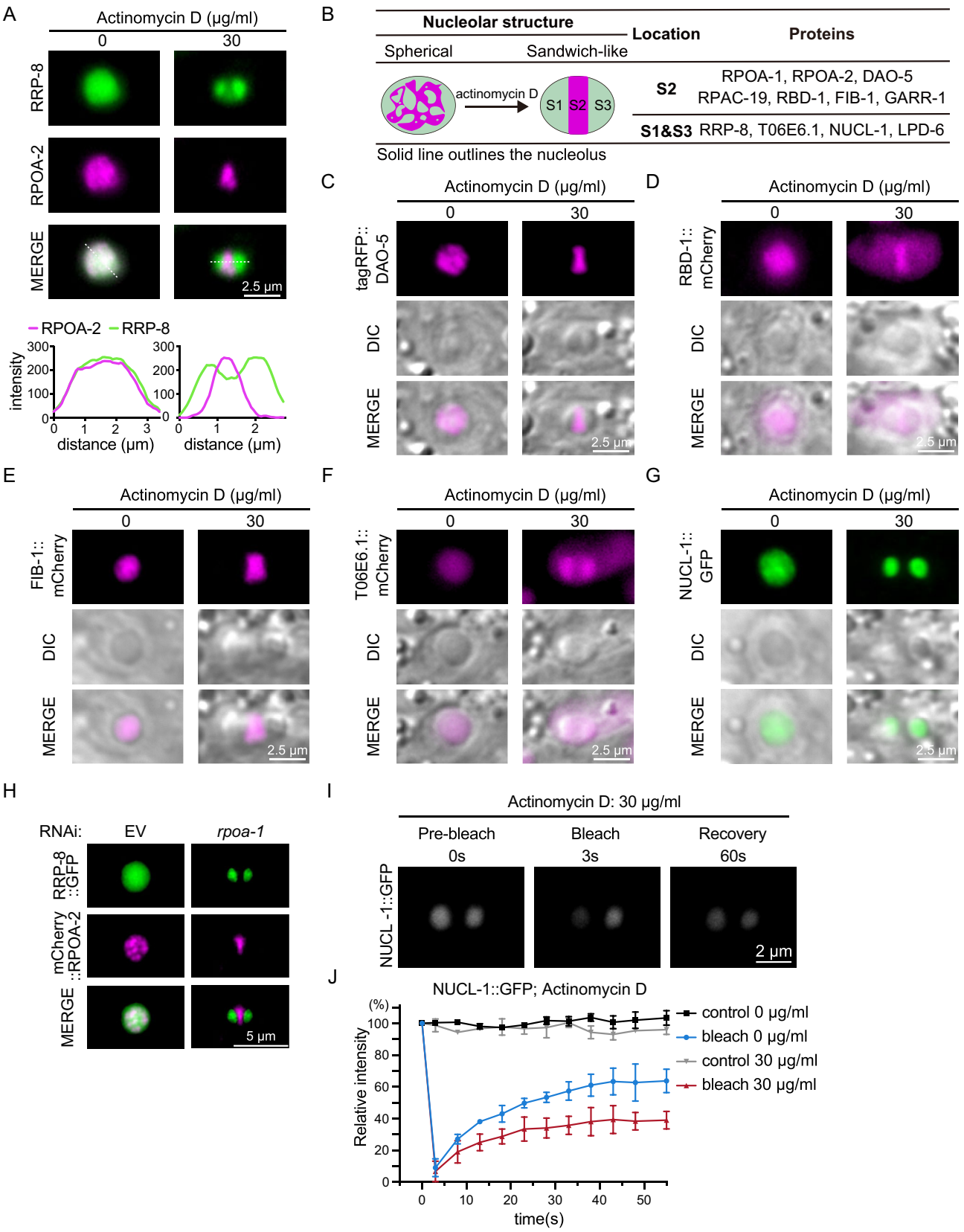

Figure 5. Inhibition of rRNA transcription induces the formation of sandwich-like nucleoli. (**A**) (top) Fluorescence microscopy images of *C. elegans* nucleoli in hypodermal cells after actinomycin D treatment for 48 h. Scale bar, 2.5 μm. (bottom) Fluorescence density scan of RRP-8::GFP and mCherry::RPOA-2 in the indicated lines via ImageJ. A line was drawn across the nucleolus, and fluorescence intensity along the line was measured to generate a profile plot. The *y*-axis represents fluorescence intensity and the *x*-axis represents the distance along the line. (**B**) Summary of the localization of the indicated proteins after actinomycin D treatment for 48 h. (**C**–**G**) DIC and fluorescence microscopy images of the indicated transgenes after actinomycin D treatment for 48 h. Scale bar, 2.5 μm. (**H**) Fluorescence microscopy images of *C. elegans* nucleoli in hypodermal cells following *rpoa-1* knockdown by RNAi. Scale bar, 5 μm. (**I**) FRAP assay of the NUCL-1::GFP transgene in the indicated regions after 30 μg/ml actinomycin D treatment for 48 h. Scale bar, 2 μm. (**J**) Quantification of FRAP data. Mean ± SD, $n = 3$ independent animals.

expressing the NUCL-1 split-GFP reporter also displayed the sandwich-like nucleolar architecture following actinomycin D treatment (Supplementary Fig. S6G).

To further test whether inhibition of rRNA transcription is sufficient to induce this structural rearrangement, we used two independent approaches to impair RNA polymerase I activity. RNAi-mediated depletion of *rpoa-1*, a subunit of the RNA polymerase I complex, and treatment with the Pol I-specific inhibitor BMH-21 [62, 63], both resulted in the formation of sandwich-like nucleoli (Fig. 5H and Supplementary Fig. S6H). Therefore, we speculate that active rRNA transcription and the presence of particular rRNA intermediates are essential for the maintenance of nucleolar architecture.

We examined protein mobility via the FRAP assay and observed a slight decrease in the mobility of NUCL-1 and GARR-1 upon actinomycin D treatment (Fig. 5I and J, and Supplementary Fig. S6I and J), suggesting a slightly more compact structure of the nucleolus upon the inhibition of rRNA transcription.

Spatial distribution of rDNA during structural reorganization of nucleoli

In addition to proteins and rRNAs, rDNA has been shown to play critical roles in nucleolar architecture as the NOR [2]. We then investigated the subcellular localization of rDNA during nucleolar structural alterations. To achieve live-cell labeling of the rDNA genome, we employed the lacI–lacO system [64–68] and ectopically inserted the lacI::tagRFP transgene into the *C. elegans* genome. Moreover, the lacO sequence was integrated into the rDNA genome via CRISPR/Cas9 technology to enable the visualization of the rDNA array by lacI::tagRFP (Fig. 6A). Notably, the *C. elegans* genome encodes ∼55 copies of a 7.2-kb tandem repeat of rDNA on LG I to express pre-rRNAs [17]. Owing to the length limitation of DNA sequencing, we are unable to determine in which specific rDNA unit the lacO sequence was inserted. To investigate the positioning of rDNA, we used a zoning assay [68–70] and examined the position of rDNA foci relative to zones C1–C3 and S1–S3 under a fluorescence microscope.

Upon *rps-8* knockdown, rDNA foci significantly accumulated in the C2 zone, in which RNAP I transcription, 18S processing, and FC region proteins were preserved (Fig. 6B–D). In actinomycin D-induced sandwich-like nucleoli, ∼90% of rDNA foci were positioned within the S2 zone (Fig. 6E–G), in which the RNAP I transcription, 18S processing, and FC region proteins were enriched as well. We did not observe pronounced accumulation of rDNA in the C1 and C3 or S1 and S3 regions (Fig. 6H and I).

Therefore, rDNA remains colocalized with rRNA transcription and 18S rRNA processing factors during nucleolar structural reorganization.

NUCL-1 is required for nucleolar reshaping

NUCL-1 in *C. elegans* encodes an evolutionarily conserved protein with high homology to nucleolin in yeast and humans. It localizes to the GC region of the nucleolus, and its N-terminal domain contains a long intrinsically disordered region with a GAR/RGG motif that is essential for its subnucleolar compartmentalization [3, 4, 14]. Our previous work revealed that NUCL-1 is required for nucleolar reshaping and NoV formation [3]. Here, we tested whether NUCL-1 is also required for nucleolar reshaping, including the formation of concentric-spherical nucleoli (type III) and the sandwich-like nucleoli (type IV).

The deletion of *nucl-1* significantly suppressed the formation of *rps-8* knockdown-induced concentric-spherical nucleoli (Fig. 7A and B). Moreover, the efficiency of *rps-8* RNAi was unaffected in the *nucl-1* mutant, indicating that the suppression was not due to impaired RNAi activity (Supplementary Fig. S7A). Notably, the deletion of *nucl-1* also prevented the formation of actinomycin D-induced sandwich-like nucleolar structures (Fig. 7C and D), but *nucl-1* mutant failed to restore pre-rRNA levels under these conditions (Supplementary Fig. S7B). In addition, *nucl-1* depletion suppressed the formation of sandwich-like nucleoli induced by *rpoa-1* knockdown (Supplementary Fig. S7C and D). Collectively, these results indicate that the absence of *nucl-1* suppresses nucleolar reshaping, including both concentric-spherical nucleoli induced by *rps-8* knockdown and sandwich-like nucleoli induced by actinomycin D treatment or *rpoa-1* RNAi. To determine whether the suppression of nucleolar reshaping in the *nucl-1* mutant was due to altered biophysical properties of the nucleolus, we performed FRAP analysis. The results indicated that nucleolar fluidity was not significantly altered in the *nucl-1* mutant (Fig. 7E and F).

cRT-PCR revealed that the deletion of NUCL-1 blocked the *rps-8*(RNAi)-induced accumulation of Ce.22SB pre-rRNA (Fig. 7G and H), further supporting a close relationship between the accumulation of Ce.22SB pre-rRNA and the formation of concentric-spherical nucleoli. To determine whether the suppressive effect of *nucl-1* extends beyond *rps-8*, we examined additional class I *rps* genes. Deletion of *nucl-1* suppressed the formation of concentric-spherical nucleoli induced by knockdown of *rps-6*, *rps-7*, and *rps-9* (Supplementary Fig. S7E and F), suggesting that *nucl-1* broadly suppresses class I RPS-mediated nucleolar reshaping.

NUCL-1, FIB-1, and LPD-6 are associated with Ce.22SB pre-rRNA accumulation during nucleolar reshaping and developmental robustness

Previous studies identified NUCL-1 as a key regulator of nucleolar sub-compartmentalization, with both FC and GC sub-compartments absent in *nucl-1* mutants [14], suggesting mixing of the FC and GC compartments [48]. NUCL-1 is a highly abundant nucleolar protein. To determine whether the suppressive effect of *nucl-1* loss on nucleolar reshaping reflects a general property of abundant nucleolar proteins or a specific role of NUCL-1, we examined additional nucleolar proteins.

According to *Spaulding et al.* [14], NUCL-1 and LPD-6 are GC-associated proteins, whereas FIB-1 and GARR-1 localize to the FC. Although GARR-1 has been implicated in nucleolar sub-compartmentalization, its depletion did not prevent the formation of concentric-spherical nucleoli or the accumulation of Ce.22SB pre-rRNA upon *rps* knockdown (Fig. 8A–D). In contrast, depletion of FIB-1 suppressed the formation of concentric nucleolar structures induced by *rps-8* knockdown, and was accompanied by reduced Ce.22SB pre-RNA levels. Although LPD-6 is unlikely to play a role in nucleolar sub-compartmentalization; its depletion suppresses both the formation of concentric-spherical nucleolar structures and the accumulation of Ce.22SB pre-rRNA upon *rps* knockdown (Fig. 8A–D). These results suggest that the effect of *nucl-1* loss cannot be solely explained by the disruption of FC/GC

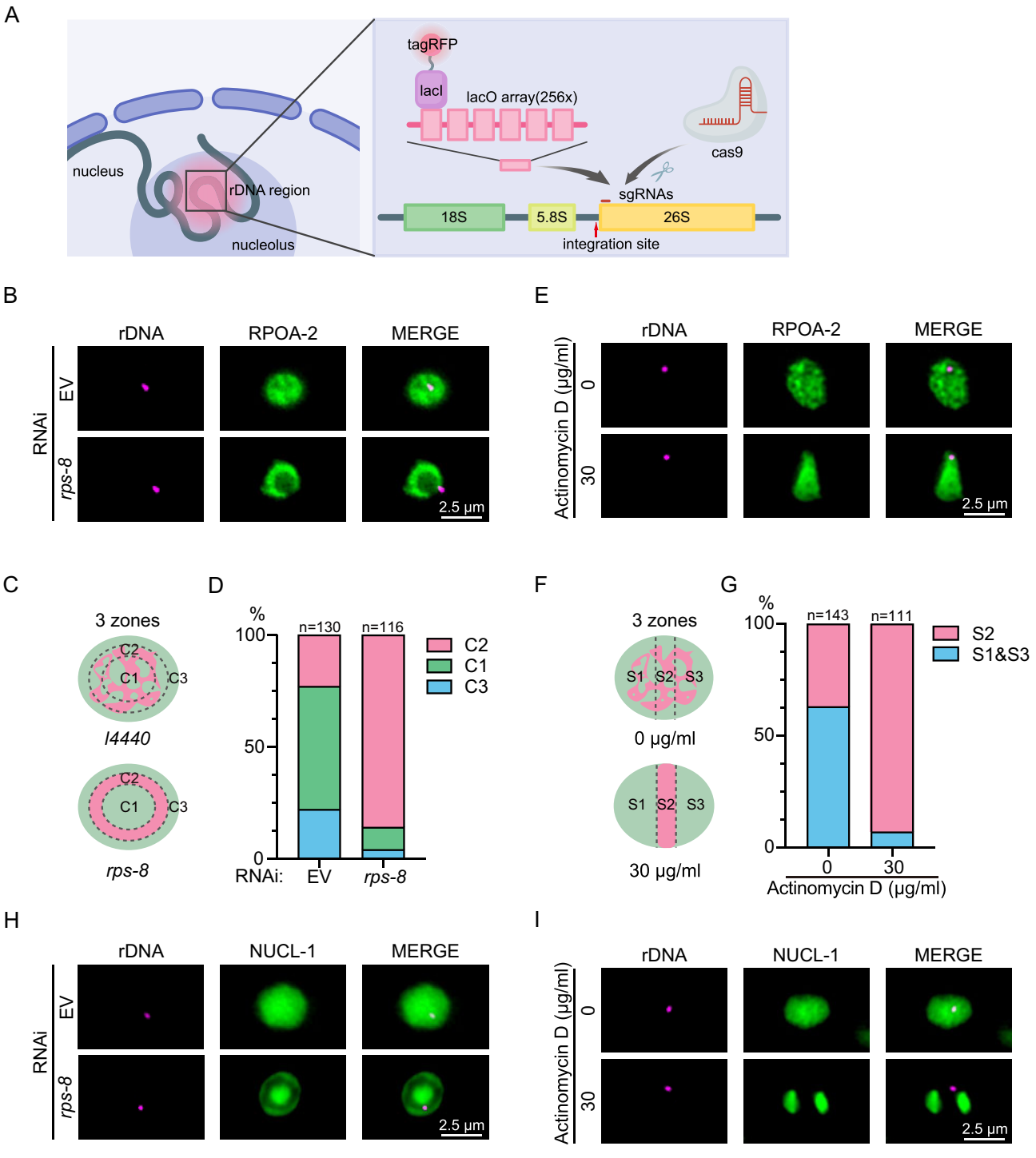

Figure 6. Localization of rDNA upon nucleolar structure reorganization. (**A**) Schematic diagram of the lacI::tagRFP/lacO system used for rDNA labeling. lacO array: 17 bp lacO + 19 bp spacer. (**B**) Fluorescence images of rDNA (labeled with lacI::tagRFP) and GFP::RPOA-2 after *rps-8* knockdown. Scale bar, 2.5 μm. RPOA-2 marks the C2 region. (**C**) Zoning assay for rDNA reporter distribution on the basis of the C1–C3 regions as defined in Fig. 1C. (**D**) Quantification of the subnucleolar distribution of rDNA. *n*, number of nucleoli. (**E**) Fluorescence microscopy images of rDNA (labeled with lacI::tagRFP) and GFP::RPOA-2 after actinomycin D treatment. Scale bar, 2.5 μm. RPOA-2 marks the S2 region. *n*, number of nucleoli. (**F**) Zoning assay using the S1–S3 regions from Fig. 5C. (**G**) Quantification of the subnucleolar distribution of rDNA. *n*, number of nucleoli. (**H**) Fluorescence microscopy images of rDNA (labeled with lacI::tagRFP) and NUCL-1 after *rps-8* knockdown. Scale bar, 2.5 μm. NUCL-1 marks the C1 and C3 region. (**I**) Fluorescence microscopy images of rDNA (labeled with lacI::tagRFP) and NUCL-1 after actinomycin D treatment. Scale bar, 2.5 μm. NUCL-1 marks the S1 and S3 region.

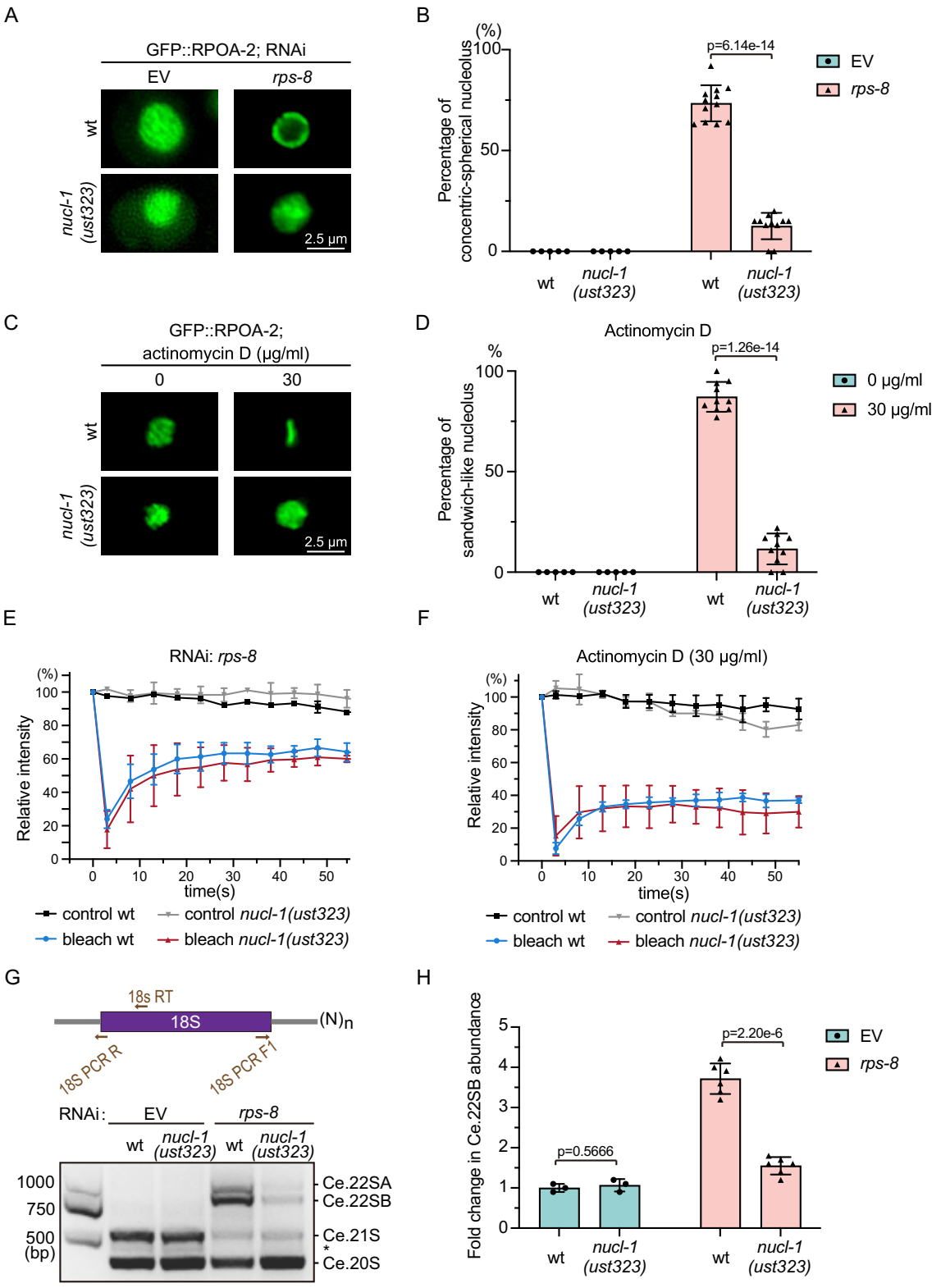

Figure 7. NUCL-1 is required for nucleolar reshaping. (**A**) Fluorescence microscopy images of GFP::RPOA-2-labled nucleoli in hypodermal cells of *C. elegans* after the indicated genes were knocked down via RNAi in wild-type (wt) and *nucl-1* mutants. Scale bar, 2.5 μm. (**B**) Quantification of concentric-spherical nucleoli cells in which the indicated genes were knocked down via RNAi in wt and *nucl-1* mutants. Mean ± SD, $n \geq 5$ independent animals. A two-tailed *t*-test was performed to determine statistical significance. (**C**) Fluorescence microscopy images of GFP::RPOA-2-labled nucleoli in hypodermal cells of *C. elegans* upon actinomycin D treatment in wt and *nucl-1* mutants. Scale bar, 2.5 μm. (**D**) Quantification of the sandwich-like nucleoli cells upon actinomycin D treatment in wt and *nucl-1* mutants. Mean ± SD, $n \geq 5$ independent animals. A two-tailed *t*-test was performed to determine statistical significance. (**E**) FRAP assay of GFP::RPOA-2 in wt and *nucl-1* mutants after *rps-8* knockdown. Mean ± SD, $n = 3$ independent animals. (**F**) FRAP assay of GFP::RPOA-2 in wt and *nucl-1* mutants after actinomycin D treatment. Mean ± SD, $n = 3$ independent animals. (**G**) cRT-PCR assay and (**H**) quantification of the Ce.22SB pre-rRNA in *nucl-1* mutants upon knockdown of the indicated genes via RNAi. Data are presented as the mean ± SD of three or six biological replicates. A two-tailed *t*-test was performed to determine statistical significance.

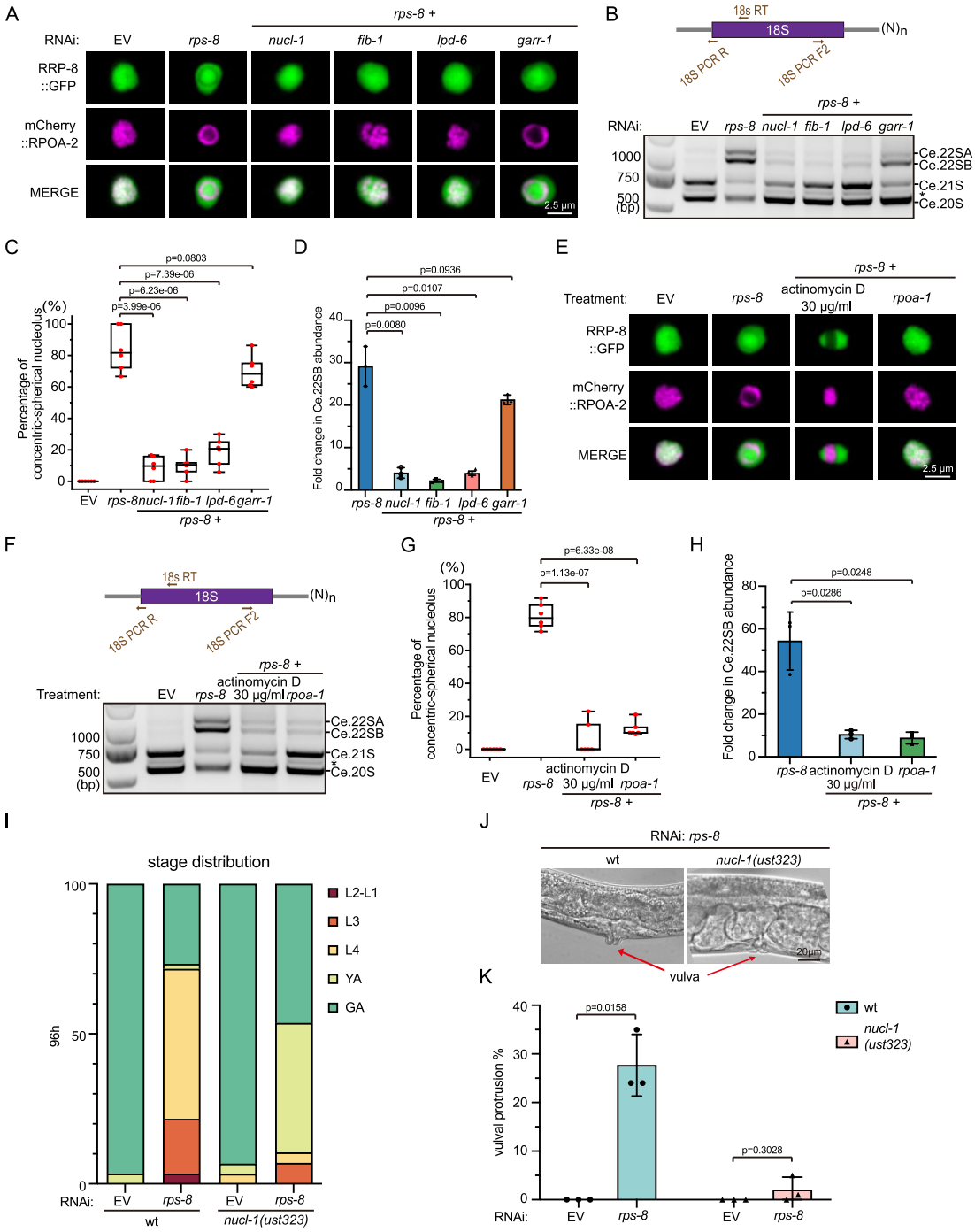

Figure 8. NUCL-1, FIB-1, and LPD-6 are associated with Ce.22SB pre-rRNA accumulation during nucleolar reshaping and developmental robustness. (**A**) Fluorescence microscopy images of nucleoli in hypodermal cells after the indicated genes were knocked down via RNAi. Scale bar, 2.5 μm. (**B**) cRT-PCR assay of pre-18S RNA after knocking down the indicated *rps* genes via RNAi. (**C**) Quantification of concentric-spherical nucleoli cells in which the indicated genes were knocked down via RNAi. Each box represents data from six worms, each dot represents the proportion of concentric-spherical nucleoli observed in at least nine individual hypodermal cells from a single worm. Significance was tested with two-tailed Student's *t*-test. (**D**) Quantification of the Ce.22SB pre-rRNA using ImageJ after knockdown of the indicated genes, normalized to the corresponding intermediate in EV RNAi controls. Data are presented as the mean ± SD of three biological replicates. A two-tailed *t*-test was performed to determine statistical significance. (**E**) Fluorescence microscopy images of nucleoli in hypodermal cells following knockdown of the indicated genes by RNAi and/or treatment with actinomycin D. Scale bar, 2.5 μm. (**F**) cRT-PCR assay of pre-18S rRNA following knockdown of the indicated genes by RNAi and/or treatment with actinomycin D. (**G**) Quantification of concentric-spherical nucleoli cells following knockdown of the indicated genes by RNAi and/or treatment with actinomycin D. Each box represents data from six worms, each dot represents the proportion of concentric-spherical nucleoli observed in at least nine individual hypodermal cells from a single worm. Significance was tested with two-tailed Student's *t*-test. (**H**) Quantification of Ce.22SB pre-rRNA using ImageJ following knockdown of the indicated genes by RNAi and/or treatment with actinomycin D, normalized to the corresponding intermediate in EV RNAi controls. Data are presented as the mean ± SD of three biological replicates. A two-tailed *t*-test was performed to determine statistical significance. (**I**) Developmental stage assessment of the indicated animals after 96 h at 20°C; $n \geq 18$ animals. (**J**) DIC images and (**K**) quantification of animals whose vulva protruded upon knocking down *rps-8* in wt and *nucl-1* mutants. (**J**) The red arrow indicates the vulva. Scale bar, 20 μm. (**K**) Mean ± SD, $n \geq 18$ animals. A two-tailed *t*-test was performed to determine statistical significance.

mixing/demixing or by the depletion of an abundant nucleolar protein.

Because nucleolar reshaping is closely associated with numerous rRNA processing factors, we next asked whether NUCL-1 directly interacts with rRNA. To address this question, we performed RIP-qPCR using NUCL-1::FLAG tagged strain. The results showed that NUCL-1 preferentially associates with pre-rRNAs rather than mature rRNA (Supplementary Fig. S8A and B). Notably, *rps-8* knockdown reduced the level of NUCL-1-associated pre-rRNAs (Supplementary Fig. S8C). Given that NUCL-1 localizes to the GC, we speculate that pre-rRNA may also present in GC region. These findings suggest that NUCL-1 may contribute to nucleolar reshaping through interactions with pre-rRNAs, rather than through nonspecific interactions with ribosomal proteins and ribosome biogenesis factors. However, further evidence will be required to determine whether this interaction is direct.

We next examined the importance of rRNA intermediates by suppressing pre-rRNA synthesis through actinomycin D treatment or RNAi knockdown of *rpoa-1*. Both perturbations effectively prevented the formation of concentric-spherical nucleoli and were accompanied by a marked reduction in Ce.22SB pre-rRNA accumulation (Fig. 8E–H), further supporting a close link between Ce.22SB pre-rRNA accumulation and the formation of concentric-spherical nucleoli. Interestingly, the two perturbations produced distinct nucleolar morphologies in the context of *rps-8* knockdown (Fig. 8E–H). Actinomycin D treatment not only inhibited concentric-spherical nucleolar formation, but also induced sandwich-like nucleoli, whereas *rpoa-1* knockdown primarily blocked the formation of concentric-spherical nucleoli without generating sandwich-like nucleolar structures. Although the mechanism underlying this difference remains unclear, one possibility is that actinomycin D causes a more complete inhibition of RNA polymerase I activity, leading to a more pronounced nucleolar reorganization.

To investigate the biological roles of NUCL-1, we examined the developmental progress of *C. elegans* upon *rps-8* knockdown with or without *nucl-1*. Depletion of *rps-8* delayed the development of nematodes, which could be partially rescued by *nucl-1* mutation (Fig. 8I). *rps-8* knockdown induced the protruding vulvar phenotype, which could also be alleviated by additional *nucl-1* mutation (Fig. 8J and K). In addition, the nucleolar proteins FIB-1 and LPD-6, similar to NUCL-1, function to promote the formation of concentric-spherical nucleoli and their depletion suppresses the *rps-8* knockdown-induced developmental delay and vulval protrusion (Supplementary Fig. S8D and E). Together, these results suggest a close association between nucleolar architecture and Ce.22SB pre-rRNA accumulation, and further support a link between nucleolar architecture and normal developmental progression.

Discussion

The nucleolus is a dynamic, multifunctional organelle that serves as the central hub for rRNA synthesis and ribosome assembly. It also participates in various cellular stress responses, including DNA damage, heat shock, transcriptional inhibition, and defects in ribosome biogenesis. Perturbations in rRNA biogenesis and ribosome production often induce marked changes in nucleolar morphology and composition [71, 72]. We previously showed that the knockdown of class I *rpl* genes in *C. elegans* leads to abnormal accumulation of $27SA_2$ pre-rRNA, and is accompanied by the formation of ring-shaped nucleoli and NoVs [3]. Here, we further investigated whether and how other perturbations of nucleolar processes influence nucleolar architecture, including pre-18S rRNA processing and rRNA transcription. We found that the knockdown of a specific subset of RPS proteins led to the accumulation of the Ce.22SB pre-rRNA, and was associated with the formation of concentric-spherical nucleoli. Similarly, the inhibition of rRNA transcription leads to the formation of another three-layered architecture, a sandwich-like nucleoli. During both modes of nucleolar structure reorganization, nucleolar proteins spatially redistribute into distinct subnucleolar regions. Furthermore, we found that *nucl-1* knockout prevents nucleolar structure reorganization. Collectively, these results reveal that diverse impairments in rRNA processing are associated with distinct alterations in nucleolar architecture, underscoring the essential contribution of rRNA biogenesis to the structural homeostasis of the nucleolus.

RPS-mediated rRNA processing is evolutionarily conserved

rRNA constitutes ∼80% of the total RNA within a cell. The production of rRNA is a complex, multistage process that involves the modification, cleavage, and folding of rRNAs with the assistance of various assembly factors, including ribosomal proteins [56, 73]. In this study, via a circular PCR-based method, we mapped the precise cleavage sites of pre-18S rRNA and identified a series of intermediates. These cleavage sites are indeed located in reported *C. elegans* rRNA processing regions, as revealed by northern blotting and primer extension methods [45, 60]. We further systematically examined the functions of RPS proteins in pre-18S rRNA processing and revealed that the depletion of a specific subset of RPS proteins led to failure of the processing steps in both the 5′ ETS and ITS1 regions and resulted in the accumulation of Ce.22SA and Ce.22SB pre-rRNAs. Interestingly, in mammalian cells, the depletion of the homologs of these RPS proteins, which are classified as i-RPSs (short for initiation-RPSs), also leads to the failure of the processing steps in the 5′ ETS and ITS1 regions and results in the accumulation of 45S and 30S pre-rRNAs [61, 74]. Although both the cleavage sites of rRNA and the sequences of rRNA intermediates in *C. elegans* are not exactly the same as those in mammalian cells are, these findings suggest that the functions of RPS proteins in pre-rRNA processing are highly conserved across species.

rRNA processing intermediates may serve as dictators of nucleolar architecture

As a multilayered membraneless structure within the cell, the nucleolus is primarily responsible for rRNA production, processing, and ribosomal assembly. Current models posit that the multilayered structure of the nucleolus may facilitate the transcription and successive processing of rRNAs [7, 75]. Nevertheless, whether and how rRNA transcription and processing regulate the layered organization of the nucleolus remain poorly understood. Recent studies have revealed that rRNA may undergo directed movement rather than passive diffusion in the nucleolus and that the sequential maturation of rRNA promotes its outward flux, suggesting that the sequential processing and advective flow of rRNA may underlie

the nucleolar form [20, 76]. Moreover, in our previous study, we showed that defects in $27SA_2$ pre-rRNA processing coordinate with the formation of vacuole-containing nucleoli in *C. elegans* [3], implying that proper rRNA processing may help shape the spatial structure of the nucleolus. Here, by systematically examining the functions of RPS proteins in the organization of nucleolar structure and pre-18S rRNA processing, we further investigated how pre-rRNA processing contributes to the multilayered organization of the nucleolus in *C. elegans*. We revealed that the depletion of class I RPS proteins leads to the formation of a concentric three-layered nucleolar architecture and the accumulation of Ce.22SA and Ce.22SB pre-rRNAs. Interestingly, although Ce.22SA and Ce.22SB pre-rRNAs contain the same 5′ ETS sequence and only differ in the 3′ ITS1 sequence, the increase of only Ce.22SA pre-rRNA does not induce noticeable nucleolar reshaping. Nevertheless, the accumulation of Ce.22SB pre-rRNA with a shorter 3′ ITS1 sequence is more closely correlated with nucleolar reshaping. We further provide multiple lines of evidence supporting a close association between Ce.22SB accumulation and the formation of concentric-spherical nucleoli. Specifically, disruption of several 40S ribosome subunit processing factors leads to Ce.22SB accumulation and concomitantly increases the frequency of concentric-spherical nucleoli. In contrast, perturbations that inhibit pre-rRNA synthesis, such as actinomycin D treatment or *rpoa-1* knockdown, prevent Ce.22SB accumulation and markedly reduce the occurrence of concentric-spherical nucleoli. Importantly, combined knockdown of *rps-8* with either *garr-1* or *lpd-6* further supports that the formation of concentric-spherical nucleoli is closely associated with Ce.22SB accumulation. Although GARR-1 exhibited a prominent nucleoplasmic signal in the EV images, the presence of full-length GFP and 3× FLAG tags may perturb its normal function or localization. Alternatively, it remains unclear whether this pattern reflects regulated localization or dynamic shuttling between subcellular compartments. Nevertheless, it is unlikely that GARR-1 is uniquely exempt from mediating nucleolar reshaping, as only a limited subset of nucleolar proteins was examined in this study. In addition, current methods for detecting nucleolar reshaping may be incomplete, and it is possible that additional types of nucleolar reorganization remain undocumented. We note that developing new approaches to express rRNA intermediates in *C. elegans* may help clarify the causal relationship between rRNA intermediates accumulation and nucleolar reshaping.

A recent study by *Quinodoz et al.* [76] has developed a very elegant method to map rRNA transcription and processing within human nucleoli. Using sequencing in parallel with imaging, they demonstrated that rRNA processing steps are spatially segregated, with sequential maturation of rRNA required for its outward movement through different nucleolar phases. They showed that defects in SSU processing can alter the ordering of nucleolar phases, resulting in inside-out nucleoli and preventing rRNA outflux, while LSU precursors are necessary to build the outermost layer of the nucleolus [76]. Whether the method could be applied in *C. elegans* requires further investigation. Although the multilayered structure of the nucleolus in nematodes is different from that in human cells, these findings suggest a potential link between specific rRNA processing events and the structural organization of the nucleolus and indicate that the regulation of nucleolar structure by pre-18S rRNA may be conserved across species. Further investigation of the effects of the disruption of specific rRNA processing steps on nucleolar structure in different organisms, including human cells, may help reveal how early pre-rRNA processing helps organize nucleolar architecture.

rRNAs are essential for sustaining nucleolar fluidity. In both *C. elegans* and mouse embryos, the inhibition of transcription leads to reduced rRNA output and a phase transition in the GC region, marked by slower diffusion and increased viscosity [77]. Changes in the phase separation properties of nucleolar subcompartments have been shown to alter nucleolar morphology and function [78]. We propose that the presence of rRNA processing intermediates may dictate the local microenvironment of the nucleolus or interact with certain nucleolar proteins in a way that changes the organization of the nucleolar structure. In human cells, the inhibition of rRNA transcription leads to the formation of nucleolar caps, reflecting segregation or redistribution of nucleolar components. In *C. elegans*, transcriptional inhibition results in the formation of sandwich-like nucleoli. This similarity between nematodes and mammals suggests that the underlying mechanism might be conserved: reduced rRNA levels alter the properties of nucleolar proteins, triggering nucleolar architecture reorganization. Therefore, rRNA is not merely a passive output of nucleolar function but also an active organizer of the nucleolar structure.

Taken together, our work reveals that changes in nucleolar morphology are tightly associated with the status of rRNA transcription and processing. However, it remains unclear whether the changes in nucleolar architecture are a manifestation of the inappropriate accumulation of rRNA processing intermediates or a result of altered viscoelastic properties of unprocessed rRNA. Given the pivotal role of rRNA intermediates in nucleolar architecture, a central unresolved question is whether specific rRNA intermediates could instruct nucleolar organization or instead accumulate as a consequence of structural reshaping. Addressing this question will require methodological advances, including the development of live-cell rRNA labeling approaches to resolve the spatial distribution and dynamics of distinct intermediates within the nucleolus. Experimentally manipulating the levels of defined rRNA intermediates in *C. elegans* could determine whether their increase is sufficient to induce nucleolar reshaping and whether different intermediates exert distinct structural effects. In parallel, *in vitro* nucleolar reconstitution using synthetic rRNA intermediates would help to assess the intrinsic capacity of individual intermediates to modulate higher-order nucleolar organization.

NUCL-1 is required for nucleolar structure reorganization

NUCL-1 is a homolog of human nucleolin (NCL) and the longest RGG domain-containing protein in the nucleolus [14]. Previous studies have shown that *nucl-1* knockout leads to delayed development after five generations [14], yet its function remains largely unclear. Here, we showed that NUCL-1 plays a crucial role in promoting nucleolar reorganization in response to impaired rRNA transcription and processing. Furthermore, we observed that *nucl-1* knockout partially reversed the *rps-8* depletion-induced delay in growth. Moreover, *nucl-1* mutation prevented the accumulation of the Ce.22SB pre-rRNA induced by *rps-8* knockdown. RIP-qPCR analysis showed that NUCL-1 preferentially associates with pre-rRNAs rather than mature rRNA and that NUCL-

1-associated pre-rRNA was reduced upon *rps-8* knockdown. These results suggest that NUCL-1 primarily interacts with rRNA intermediates and that this interaction is sensitive to perturbations in ribosomal protein function. The reduced association following *rps-8* depletion may reflect altered availability, processing, or structural organization of pre-rRNA substrates within nucleoli. Taken together, these findings support a model in which NUCL-1 is functionally linked to pre-rRNA metabolism and contributes to nucleolar reshaping through its interaction with pre-rRNA. We speculated that the nucleolar architecture is not only shaped by rRNA processing but also feeds back to influence rRNA maturation via NUCL-1. Notably, NUCL-1 may act as a checkpoint of rRNA processing, thereby ensuring the fidelity of ribosome biogenesis.

Intriguingly, haploinsufficiency of ribosomal protein (RP) genes leads to ribosomopathies in humans, such as Diamond–Blackfan anemia (DBA) [79] and acute myeloid leukemia (AML), for which effective therapies are still lacking. These ribosomopathies are frequently linked to dysregulated rRNA processing [80–84]. For example, mutation of the DBA gene *rps7* leads to the accumulation of the 30S rRNA intermediate [83], indicating failure of 5′ ETS cleavage. Our work highlights NUCL-1/NCL as a potential regulatory node in this process and underscores the importance of nucleolar architecture in maintaining rRNA and ribosome homeostasis. Further investigation into the mechanistic interplay between rRNA processing, nucleolar morphology, and developmental processes may yield novel insights and therapeutic avenues for ribosomopathies.

Acknowledgements

We are grateful to the members of the Guang laboratory for their comments and suggestions. We are grateful to the International *C. elegans* Gene Knockout Consortium and the National Bioresource Project for providing the strains. Some strains were provided by the CGC, which is funded by the NIH Office of Research Infrastructure Programs (P40 OD010440).

Author contributions: S.G., X.F., X.C., and J.C. conceptualized the research; Xinya Huang, X.C., C.Z., X.F., and S.G. designed the research; J.C., L.L., D.X., Y.C.,Y.K., A.Z., M.H., Xiaona Huang, X.Z., W.N., J.Z. and Xinya Huang performed the research; J.C., L.L., D.X., Y.C., and Y.K. contributed new reagents; J.C., X.C., X.F., and S.G. wrote the paper.

Supplementary data

Supplementary data is available at NAR online.

Conflict of interest

None declared.

Funding

This work was supported by grants from the National Natural Science Foundation of China (32230016, 32270583, 32300438, 32400435, and 32470633), the National Key R&D Program of China (2022YFA1302700), the Research Funds of Center for Advanced Interdisciplinary Science and Biomedicine of IHM (QYPY20230021), and the Fundamental Research Funds for the Central Universities. This study was also supported in part by the China Postdoctoral Science Foundation under Grant Number 2023M733425.

Data availability

The data underlying this article are available in the article and in its online supplementary material.

References

1. Pederson T. The nucleolus. *Cold Spring Harb Perspect Biol* 2011;3:a000638. https://doi.org/10.1101/cshperspect.a000638
2. McStay B. Nucleolar organizer regions: genomic 'dark matter' requiring illumination. *Genes Dev.* 2016;30:1598–610. https://doi.org/10.1101/gad.283838.116
3. Xu D, Chen X, Kuang Y *et al.* rRNA intermediates coordinate the formation of nucleolar vacuoles in *C. elegans*. *Cell Rep* 2023;42:112915. https://doi.org/10.1016/j.celrep.2023.112915
4. Hong M, Zhou X, Zeng C *et al.* Nucleolar stress induces nucleolar stress body formation via the NOSR-1/NUMR-1 axis in *Caenorhabditis elegans*. *Nat Commun* 2024;15:7256. https://doi.org/10.1038/s41467-024-51693-z
5. Bohnsack KE, Bohnsack MT. Uncovering the assembly pathway of human ribosomes and its emerging links to disease. *EMBO J* 2019;38:e100278. https://doi.org/10.15252/embj.2018100278
6. Cenik ES, Meng X, Tang NH *et al.* Maternal ribosomes are sufficient for tissue diversification during embryonic development in *C. elegans*. *Dev Cell* 2019;48:811–826.e6. https://doi.org/10.1016/j.devcel.2019.01.019
7. Lafontaine DLJ, Riback JA, Bascetin R *et al.* The nucleolus as a multiphase liquid condensate. *Nat Rev Mol Cell Biol* 2021;22:165–82. https://doi.org/10.1038/s41580-020-0272-6
8. Tartakoff A, Dimario P, Hurt E *et al.* The dual nature of the nucleolus. *Genes Dev.* 2022;36:765–9. https://doi.org/10.1101/gad.349748.122
9. Kruger T, Zentgraf H, Scheer U. Intranucleolar sites of ribosome biogenesis defined by the localization of early binding ribosomal proteins. *J Cell Biol* 2007;177:573–8. https://doi.org/10.1083/jcb.200612048
10. Shaw PJ, Brown JW. Plant nuclear bodies. *Curr Opin Plant Biol* 2004;7:614–20. https://doi.org/10.1016/j.pbi.2004.09.011
11. Brown JW, Shaw PJ. The role of the plant nucleolus in pre-mRNA processing. *Curr Top Microbiol Immunol* 2008;326:291–311.
12. Kalinina NO, Makarova S, Makhotenko A *et al.* The Multiple functions of the nucleolus in plant development, disease and stress responses. *Front Plant Sci* 2018;9:132. https://doi.org/10.3389/fpls.2018.00132
13. Knibiehler B, Mirre C, Rosset R. Nucleolar organizer structure and activity in a nucleolus without fibrillar centres: the nucleolus in an established *Drosophila* cell line. *J Cell Sci* 1982;57:351–64. https://doi.org/10.1242/jcs.57.1.351
14. Spaulding EL, Feidler AM, Cook LA *et al.* RG/RGG repeats in the *C. elegans* homologs of nucleolin and GAR1 contribute to sub-nucleolar phase separation. *Nat Commun* 2022;13:6585. https://doi.org/10.1038/s41467-022-34225-5
15. Moraleva AA, Deryabin AS, Rubtsov YP *et al.* Eukaryotic ribosome biogenesis: the 40S Subunit. *Acta Naturae* 2022;14:14–30. https://doi.org/10.32607/actanaturae.11540
16. Spirin AS. Ribosome as a molecular machine. *FEBS Lett* 2002;514:2–10. https://doi.org/10.1016/S0014-5793(02)02309-8
17. Lee LW, Lee CC, Huang CR *et al.* The nucleolus of *Caenorhabditis elegans*. *J Biomed Biotechnol* 2012;2012:1. https://doi.org/10.1155/2012/601274
18. Mougey EB, O'Reilly M, Osheim Y *et al.* The terminal balls characteristic of eukaryotic rRNA transcription units in chromatin spreads are rRNA processing complexes. *Genes Dev* 1993;7:1609–19. https://doi.org/10.1101/gad.7.8.1609

19. Miller OL, Beatty BR. Visualization of nucleolar genes. *Science* 1969;164:955–7. https://doi.org/10.1126/science.164.3882.955
20. Riback JA, Eeftens JM, Lee DSW *et al.* Viscoelasticity and advective flow of RNA underlies nucleolar form and function. *Mol Cell* 2023;83:3095–3107.e9. https://doi.org/10.1016/j.molcel.2023.08.006
21. Huang S. Building an efficient factory: where is pre-rRNA synthesized in the nucleolus? *J Cell Biol* 2002;157:739–41. https://doi.org/10.1083/jcb.200204159
22. Ban N, Nissen P, Hansen J *et al.* The complete atomic structure of the large ribosomal subunit at 2.4 Å resolution. *Science* 2000;289:905–20. https://doi.org/10.1126/science.289.5481.905
23. Jenner L, Melnikov S, Garreau de Loubresse N *et al.* Crystal structure of the 80S yeast ribosome. *Curr Opin Struct Biol* 2012;22:759–67. https://doi.org/10.1016/j.sbi.2012.07.013
24. Klinge S, Voigts-Hoffmann F, Leibundgut M *et al.* Atomic structures of the eukaryotic ribosome. *Trends Biochem Sci* 2012;37:189–98. https://doi.org/10.1016/j.tibs.2012.02.007
25. Melnikov S, Ben-Shem A, Garreau De Loubresse N *et al.* One core, two shells: bacterial and eukaryotic ribosomes. *Nat Struct Mol Biol* 2012;19:560–7. https://doi.org/10.1038/nsmb.2313
26. Dörner K, Ruggeri C, Zemp I *et al.* Ribosome biogenesis factors—from names to functions. *EMBO J* 2023;42:e112699.
27. Reynolds RC, Montgomery PO, Hughes B. Nucleolar 'caps' produced by actinomycin D. *Cancer Res* 1964;24:1269–77.
28. Shav-Tal Y, Blechman J, Darzacq X *et al.* Dynamic sorting of nuclear components into distinct nucleolar caps during transcriptional inhibition. *Mol Biol Cell* 2005;16:2395–413. https://doi.org/10.1091/mbc.e04-11-0992
29. Ye S, Latham AP, Tang Y *et al.* Micropolarity governs the structural organization of biomolecular condensates. *Nat Chem Biol* 2023;20:443–451.
30. Montanaro L, Treré D, Derenzini M. Nucleolus, ribosomes, and cancer. *Am J Pathol* 2008;173:301–10. https://doi.org/10.2353/ajpath.2008.070752
31. Corman A, Sirozh O, Lafarga V *et al.* Targeting the nucleolus as a therapeutic strategy in human disease. *Trends Biochem Sci* 2023;48:274–87. https://doi.org/10.1016/j.tibs.2022.09.006
32. Timmons L, Court DL, Fire A. Ingestion of bacterially expressed dsRNAs can produce specific and potent genetic interference in *Caenorhabditis elegans*. *Gene* 2001;263:103–12. https://doi.org/10.1016/S0378-1119(00)00579-5
33. Kamath RS, Fraser AG, Dong Y *et al.* Systematic functional analysis of the *Caenorhabditis elegans* genome using RNAi. *Nature* 2003;421:231–7. https://doi.org/10.1038/nature01278
34. Chen X, Liao S, Huang X *et al.* Targeted chromosomal rearrangements via combinatorial use of CRISPR/Cas9 and Cre/LoxP technologies in *Caenorhabditis elegans*. *G3 (Bethesda)* 2018;8:2697–707. https://doi.org/10.1534/g3.118.200473
35. Frøkjaer-Jensen C, Davis MW, Hopkins CE *et al.* Single-copy insertion of transgenes in *Caenorhabditis elegans*. *Nat Genet* 2008;40:1375–83. https://doi.org/10.1038/ng.248
36. Huang X, Cheng P, Weng C *et al.* A chromodomain protein mediates heterochromatin-directed piRNA expression. *Proc Natl Acad Sci USA* 2021;118:e2103723118. https://doi.org/10.1073/pnas.2103723118
37. Zhu C, Yan Q, Weng C *et al.* Erroneous ribosomal RNAs promote the generation of antisense ribosomal siRNA. *Proc Natl Acad Sci USA* 2018;115:10082–7. https://doi.org/10.1073/pnas.1800974115
38. Dauwerse JG, Dixon J, Seland S *et al.* Mutations in genes encoding subunits of RNA polymerases I and III cause Treacher Collins syndrome. *Nat Genet* 2011;43:20–2. https://doi.org/10.1038/ng.724
39. Hedgecock EM, White JG. Polyploid tissues in the nematode *Caenorhabditis elegans*. *Dev Biol* 1985;107:128–33. https://doi.org/10.1016/0012-1606(85)90381-1
40. Guang S, Bochner AF, Burkhart KB *et al.* Small regulatory RNAs inhibit RNA polymerase II during the elongation phase of transcription. *Nature* 2010;465:1097–101. https://doi.org/10.1038/nature09095
41. Liao S, Chen X, Xu T *et al.* Antisense ribosomal siRNAs inhibit RNA polymerase I-directed transcription in *C. elegans*. *Nucleic Acids Res* 2021;49:9194–210. https://doi.org/10.1093/nar/gkab662
42. Burkhart KB, Guang S, Buckley BA *et al.* A Pre-mRNA–associating factor links endogenous siRNAs to chromatin regulation. *PLoS Genet* 2011;7:e1002249. https://doi.org/10.1371/journal.pgen.1002249
43. Hang R, Wang Z, Deng X *et al.* Ribosomal RNA Biogenesis and Its Response to Chilling Stress in *Oryza sativa*. *Plant Physiol.* 2018;177:381–97. https://doi.org/10.1104/pp.17.01714
44. Lee CC, Tsai YT, Kao CW *et al.* Mutation of a Nopp140 gene dao-5 alters rDNA transcription and increases germ cell apoptosis in *C. elegans*. *Cell Death Dis* 2014;5:e1158. https://doi.org/10.1038/cddis.2014.114
45. Saijou E. RBD-1, a nucleolar RNA-binding protein, is essential for *Caenorhabditis elegans* early development through 18S ribosomal RNA processing. *Nucleic Acids Res* 2004;32:1028–36. https://doi.org/10.1093/nar/gkh264
46. Tollervey D, Lehtonen H, Jansen R *et al.* Temperature-sensitive mutations demonstrate roles for yeast fibrillarin in pre-rRNA processing, pre-rRNA methylation, and ribosome assembly. *Cell* 1993;72:443–57. https://doi.org/10.1016/0092-8674(93)90120-F
47. Tollervey D, Lehtonen H, Carmo-Fonseca M *et al.* The small nucleolar RNP protein NOP1 (fibrillarin) is required for pre-rRNA processing in yeast. *Embo J* 1991;10:573–83. https://doi.org/10.1002/j.1460-2075.1991.tb07984.x
48. Spaulding EL, Updike DL. Intrinsically disordered arginine-glycine repeat domains tune sub-nucleolar compartmentalization in *Caenorhabditis elegans*. *Genetics* 2025;230:iyaf067. https://doi.org/10.1093/genetics/iyaf067
49. Yokoyama W, Hirota K, Wan H *et al.* rRNA adenine methylation requires T07A9.8 gene as rram-1 in *Caenorhabditis elegans*. *J Biochem* 2018;163:465–74. https://doi.org/10.1093/jb/mvy018
50. Hiraishi N, Ishida YI, Sudo H *et al.* WDR74 participates in an early cleavage of the pre-rRNA processing pathway in cooperation with the nucleolar AAA-ATPase NVL2. *Biochem Biophys Res Commun* 2018;495:116–23. https://doi.org/10.1016/j.bbrc.2017.10.148
51. Suzuki K, Tsunekawa Y, Hernandez-Benitez R *et al. In vivo* genome editing via CRISPR/Cas9 mediated homology-independent targeted integration. *Nature* 2016;540:144–9. https://doi.org/10.1038/nature20565
52. Pfister AS, Keil M, Kuhl M. The Wnt target protein peter pan defines a novel p53-independent nucleolar stress-response pathway. *J Biol Chem* 2015;290:10905–18. https://doi.org/10.1074/jbc.M114.634246
53. Fatica A, Cronshaw AD, Dlakić M *et al.* Ssf1p prevents premature processing of an early pre-60S ribosomal particle. *Mol Cell* 2002;9:341–51. https://doi.org/10.1016/S1097-2765(02)00458-6
54. Kim J, Hirsch JP. A nucleolar protein that affects mating efficiency in *Saccharomyces cerevisiae* by altering the morphological response to pheromone. *Genetics* 1998;149:795–805. https://doi.org/10.1093/genetics/149.2.795
55. Nicolas E, Parisot P, Pinto-Monteiro C *et al.* Involvement of human ribosomal proteins in nucleolar structure and p53-dependent nucleolar stress. *Nat Commun* 2016;7:11390. https://doi.org/10.1038/ncomms11390
56. Klinge S, Woolford JL. Ribosome assembly coming into focus. *Nat Rev Mol Cell Biol* 2019;20:116–31. https://doi.org/10.1038/s41580-018-0078-y
57. Bleichert F, Granneman S, Osheim YN *et al.* The PINc domain protein Utp24, a putative nuclease, is required for the early cleavage steps in 18S rRNA maturation. *Proc Natl Acad Sci USA* 2006;103:9464–9. https://doi.org/10.1073/pnas.0603673103
58. Tomecki R, Sikorski PJ, Zakrzewska-Placzek M. Comparison of preribosomal RNA processing pathways in yeast, plant and

human cells—focus on coordinated action of endo- and exoribonucleases. *FEBS Lett* 2017;591:1801–50. https://doi.org/10.1002/1873-3468.12682
59. An W, Yan Y, Ye K. High resolution landscape of ribosomal RNA processing and surveillance. *Nucleic Acids Res* 2024;52:10630–44. https://doi.org/10.1093/nar/gkae606
60. Shovon SR, Uematsu T, Osaki Y *et al.* Starvation changes the pre-rRNA accumulations in *Caenorhabditis elegans*. *Biochem Biophys Res Commun* 2025;742:151125. https://doi.org/10.1016/j.bbrc.2024.151125
61. O'Donohue M-F, Choesmel V, Faubladier M *et al.* Functional dichotomy of ribosomal proteins during the synthesis of mammalian 40S ribosomal subunits. *J Cell Biol* 2010;190:853–66.
62. Jacobs RQ, Fuller KB, Cooper SL *et al.* RNA polymerase I is uniquely vulnerable to the small-molecule inhibitor BMH-21. *Cancers* 2022;14:5544, https://doi.org/10.3390/cancers14225544
63. Wei T, Najmi SM, Liu H *et al.* Small-molecule targeting of RNA polymerase i activates a conserved transcription elongation checkpoint. *Cell Rep* 2018;23:404–14. https://doi.org/10.1016/j.celrep.2018.03.066
64. Robinett CC, Straight A, Li G *et al.* *In vivo* localization of DNA sequences and visfalization of large-scale chromatin organization using lac operator/repressor recognition. *J Cell Biol* 1996;135:1685–700. https://doi.org/10.1083/jcb.135.6.1685
65. Carmi I, Kopczynski JB, Meyer BJ. The nuclear hormone receptor SEX-1 is an X-chromosome signal that determines nematode sex. *Nature* 1998;396:168–73. https://doi.org/10.1038/24164
66. Kaltenbach L, Horner MA, Rothman JH *et al.* The TBP-like factor CeTLF is required to activate RNA polymerase II transcription during *C. elegans* embryogenesis. *Mol Cell* 2000;6:705–13. https://doi.org/10.1016/S1097-2765(00)00068-X
67. Gonzalez-Serricchio AS, Sternberg PW. Visualization of *C. elegans* transgenic arrays by GFP. *BMC Genet* 2006;7:36. https://doi.org/10.1186/1471-2156-7-36
68. Meister P, Towbin BD, Pike BL *et al.* The spatial dynamics of tissue-specific promoters during *C. elegans* development. *Genes Dev.* 2010;24:766–82. https://doi.org/10.1101/gad.559610
69. Meister P, Gehlen LR, Varela E *et al.* Visualizing yeast chromosomes and nuclear architecture. *Methods Enzymol* 2010;470:535–67.
70. Al-Refaie N, Padovani F, Hornung J *et al.* Fasting shapes chromatin architecture through an mTOR/RNA Pol I axis. *Nat Cell Biol* 2024;26:1903–17. https://doi.org/10.1038/s41556-024-01512-w
71. Feric M, Vaidya N, Harmon TS *et al.* Coexisting liquid phases underlie nucleolar subcompartments. *Cell* 2016;165:1686–97. https://doi.org/10.1016/j.cell.2016.04.047
72. Potapova TA, Unruh JR, Conkright-Fincham J *et al.* Distinct states of nucleolar stress induced by anticancer drugs. *eLife* 2023;12:RP88799. https://doi.org/10.7554/eLife.88799
73. Henras AK, Plisson-Chastang C, O'Donohue MF *et al.* An overview of pre-ribosomal RNA processing in eukaryotes. *WIREs RNA* 2015;6:225–42. https://doi.org/10.1002/wrna.1269
74. Tafforeau L, Zorbas C, Langhendries J-L *et al.* The complexity of human ribosome biogenesis revealed by systematic nucleolar screening of pre-rRNA processing factors. *Mol Cell* 2013;51:539–51. https://doi.org/10.1016/j.molcel.2013.08.011
75. Pan YH, Shan L, Yang ZH *et al.* Pre-rRNA spatial distribution and functional organization of the nucleolus. *Nature* 2025;646:227–35. https://doi.org/10.1101/2024.11.02.621631
76. Quinodoz SA, Jiang L, Abu-Alfa AA *et al.* Mapping and engineering RNA-controlled architecture of the multiphase nucleolus. *Nature* 2025;644:557–66.
77. Dash S, Lamb MC, Lange JJ *et al.* rRNA transcription is integral to phase separation and maintenance of nucleolar structure. *PLoS Genet* 2023;19:e1010854. https://doi.org/10.1371/journal.pgen.1010854
78. Zhu L, Richardson TM, Wacheul L *et al.* Controlling the material properties and rRNA processing function of the nucleolus using light. *Proc Natl Acad Sci USA* 2019;116:17330–5. https://doi.org/10.1073/pnas.1903870116
79. Surya A, Bolton BM, Rothe R *et al.* Differential impacts of ribosomal protein haploinsufficiency on mitochondrial function. *J Cell Biol* 2025;224;e202404084. https://doi.org/10.1083/jcb.202404084
80. Paolini NA, Attwood M, Sondalle SB *et al.* A ribosomopathy reveals decoding defective ribosomes driving human dysmorphism. *Am Hum Genet* 2017;100:506–22. https://doi.org/10.1016/j.ajhg.2017.01.034
81. Ulirsch JC, Verboon JM, Kazerounian S *et al.* The genetic landscape of Diamond-Blackfan anemia. *Am Hum Genet* 2018;103:930–47. https://doi.org/10.1016/j.ajhg.2018.10.027
82. Goudarzi KM, Lindström MS. Role of ribosomal protein mutations in tumor development (Review). *Int J Oncol* 2016;48:1313–24. https://doi.org/10.3892/ijo.2016.3387
83. Watkins-Chow DE, Cooke J, Pidsley R *et al.* Mutation of the Diamond-Blackfan anemia gene Rps7 in mouse results in morphological and neuroanatomical phenotypes. *PLoS Genet* 2013;9:e1003094. https://doi.org/10.1371/journal.pgen.1003094
84. Farrar JE, Nater M, Caywood E *et al.* Abnormalities of the large ribosomal subunit protein, Rpl35a, in Diamond-Blackfan anemia. *Blood* 2008;112:1582–92. https://doi.org/10.1182/blood-2008-02-140012

Received: August 28, 2025. **Revised:** May 21, 2026. **Accepted:** May 26, 2026